

THE EFFECT OF PARTIAL REDISTRIBUTION ON SPECTRAL LINE FORMATION

A Thesis
Submitted For the Degree of
Doctor of Philosophy in The Faculty of Science
PUNJABI UNIVERSITY
PATIALA

By
K.E.RANGARAJAN

INDIAN INSTITUTE OF ASTROPHYSICS
BANGALORE 560034
INDIA

DECEMBER 1987

DEDICATION

I dedicate this thesis to the memory of
my parents.

ACKNOWLEDGEMENTS

The useful guidance of Prof A.Peraiah throughout this work helped me to a great extent. He tolerated many of my mistakes and his teaching gave me the necessary encouragement. It is a pleasure to acknowledge Prof H.S.Gurm, Punjabi University, Patiala for his keen interest in my work. I am indebted to Prof J.C.Bhattacharyya, the Director, Indian institute of Astrophysics for allowing me virtually unlimited computer time and the financial assistance. I am grateful to Prof M.K.V.Bappu and Mrs Yamuna Bappu for the encouragement they gave me especially in the early stage of my career as a research student.

Mr.M.Srinivasa Rao, Mr.B.A.Varghese and Mr.K.B.Ramesh worked very hard to see to the completion of this thesis. The moral support which is essential was provided by Dr.K.N.Nagendra.

The computational work which forms the major part of this thesis would not have been possible without the help of Dr.K.K.Ghosh, Dr.Sunetra Giridhar and Mr Chandra mouli. Most of the analysis is the outcome of the discussions which I had with Mr.D.Mohan Rao.

I am unable to find words to thank Dr.N.Gopaldaswamy, Mr.G.Thejappa and an unknown referee who suggested many changes and corrections in the preparation of this manuscript.

The help of the library staff had been immense. The draughtsmanship of Mr.S.Muthukrishnan can be seen in many of the complicated figures. Mr.Arvind paranjpye reduced the graphs photographically. The copies had to be taken by Mr.A.Elangovan who had to work till the late hours of the day. Binding work was done in a record time by binding section staff whose keen interest in this matter is gratefully acknowledged.

I would like to thank my siblings for their patience and Mr.G.Chakravarthy for the financial help.

Finally I would like to thank all those whose names are not mentioned but who nevertheless had helped me in this endeavour.

CONTENTS

	<u>page</u>
ABSTRACT	I-III
Chapter 1 ... INTRODUCTION ..	1-7
1.1 Why study spectral lines? ..	1
1.2 Method employed to solve transfer equation ..	1
1.3 Description of the problems in this study. ..	3
Chapter 2 ... THE EFFECT OF THE PARTIAL FREQUENCY REDISTRIBUTION FUNCTIONS R_I , R_{II} , R_{III} AND R_V ON THE SPECTRAL LINE FORMATION. ..	8-44
2.1 Introduction ..	8
2.2 Redistribution functions. ..	11
2.3 Basic equations and the computational procedure. ..	30
2.4 Results and discussion. ..	31
Chapter 3 ... THE EFFECT OF COHERENT AND NON- COHERENT ELECTRON SCATTERING WITH ATOMIC PARTIAL FREQUENCY REDISTRIBUTION ON LINE FORMATION ..	45-74
3.1 Introduction ..	45

CONTENTS

	<u>page</u>
3.2 Electron redistribution function ..	47
3.3 Method of solution ..	51
3.4 Results and discussion ..	67
Chapter 4 ... EFFECT OF EMISSION PROFILE ON LINE FORMATION ..	75-89
4.1 Introduction ..	75
4.2 The source function including the emission profile ..	77
4.3 Results and discussion ..	87
Chapter 5 ... EFFECT OF SMALL MACROSCOPIC VELOCITIES ON Ca II H AND K LINES. ..	90-106
5.1 Introduction ..	90
5.2 Atomic model ..	92
5.3 Computational procedure ..	95
5.4 Results ..	102
Chapter 6 ... CONCLUSIONS AND FUTURE WORK ..	107-110
6.1 Summary of the results ..	107
6.2 Future work ..	109
REFERENCES ...	111-114

ABSTRACT

The main effort of this study is concentrated on ascertaining the role of partial redistribution (PRD) functions in the process of spectral line formation. The effects of angle averaged R_I, R_{II}, R_{III} and R_V redistribution with isotropic phase function are studied. We have compared these results with those obtained using complete redistribution (CRD). Transfer equation with plane parallel geometry is solved using the Discrete space theory technique of Grant and Hunt (1969). Various types of boundary conditions are considered. The following results are the new and important conclusions of this study.

In this study, we find that for a purely scattering optically thick medium, R_I function produces deeper absorption profile compared to other functions. The redistribution function R_{II} is more coherent than R_V and R_V is more coherent than R_{III} in the wings. The more non-coherent the redistribution function is, the higher would be the emergent intensity in the Doppler core. If thermal sources are present in the medium and if there is incident radiation on the lower boundary, all the redistribution functions give the same intensity in the core. But in the wings, the more non-coherent the redistribution is, the higher would be the intensity. The presence of continuous opacity makes the spectral lines appear weak. Their effects are more pronounced compared to that of the

thermal sources in the medium and are present for any type of redistribution mechanism. In high optical depth situations, the R_{III} type of redistribution allows the photons to diffuse to the line centre and increase the intensity there.

In the third chapter, coherent and non-coherent electron scattering combined with complete and partial redistribution by atoms are studied for some parametrized models. Since this problem is characterized by two frequency scales, one for the atoms and the other for the electrons, two types of frequency quadrature are required to cover the effect of both the processes. Though the basic equations are solved within the framework of Discrete space theory, the frequency quadrature points, normalization, segmenting the problem into core and wing regions and the iteration procedure all follow that of Auer and Mihalas (1968). We obtain the following new result: If the coherent electron scattering is the only continuous opacity source, we find that the more non-coherent the redistribution by atoms is, the higher the value of the mean intensity in the wings for optically thick media. The non-coherent electron scattering combined with PRD fills up the core and hence one gets higher fluxes in the core compared to coherent electron scattering.

We investigate the deviation of absorption and emission profiles from each other for a two level atom with angle averaged redistribution functions. The correct expression for the source function derived by Baschek, Mihalas

and Oxenius (1981) is used to solve consistently for the emission profile and the radiation field. From this study, we get the following new and important results: The absorption and emission profiles do not deviate from each other in the Doppler core for any redistribution function even if the stimulated emission term is important. The deviation of absorption and emission profiles in the wing is more for coherent type of redistribution function. R_{III} redistribution gives identical absorption and emission profiles and so one can approximate R_{III} by CRD for all practical purposes.

The effects of small macroscopic velocity fields on Ca II H and K lines are given in chapter 5. The atomic model chosen contains the lower most five levels and the continuum. radiative transfer equation and statistical equilibrium equations are solved simultaneously using equivalent two level atom method. A schematic chromospheric type of atmosphere is considered. The emergent profiles are calculated for the systematic expanding velocities 0.0, 0.5 and 1.0 (velocities at the outer boundaries expressed in mean thermal units). We obtain the following significant results: Even though the velocities are small, they seem to affect the shapes of the H and K profiles considerably. A single peak emission instead of a double-peaked emission is obtained for the K line with $v = 1$ and $\mu = 0.79$. ($\mu = \cos\theta$, θ is the angle of the ray to the normal at the surface.). The small velocities do not affect the infrared triplet lines significantly.

CHAPTER 1

INTRODUCTION

1.1 Why study spectral lines ?

Ever since Fraunhofer obtained the solar spectrum, the study of spectral lines became one of the major activities of Astrophysics. It has been realised that the study of spectral lines is a valuable diagnostic tool to infer the physical conditions of the gaseous material present in the stars. The long column densities, low pressures and large temperature gradients are some of the unique features akin to the stellar atmospheres. Though excellent text books, review articles and research papers have been written on this topic, it still remains as an exciting field due to the variety of physical conditions which the celestial bodies offer. The spectra of Quasars, Seyfert galaxies, Wolf-Rayet stars are to name, a few of the observations which open new avenues into the study of Astronomy. Wilson-Bappu effect still remains as an enigma. From all these one can conclude that there is a compelling reason to study spectral line formation.

1.2 Method employed to solve the transfer equation.

The radiative transport in spectral lines is described

by the radiative transfer equation which is an integro-differential equation with two point boundary conditions for simple plane parallel geometry and steady state situation. Several numerical methods exist to solve this equation each one having its own advantages and disadvantages. These methods are described in a book titled 'Methods in radiative transfer' edited by Kalkofen (1984).

Ambartzumian (1942) enunciated the principle of invariance in semi-infinite homogeneous media. This was later extended to finite, homogeneous plane parallel scattering media by Chandrasekhar (1950), which helped in solving large class of problems involving the radiative transfer. Following Wick (1943), Chandrasekhar also replaced the scattering integral by a discrete sum and solved the resulting system of linear differential equations. This formed the basis for most of the subsequent work in radiative transfer theory.

Using Discrete space theory technique developed by Redheffer (1962), Preisendorfer (1965) and Van de Hulst (1965), Grant and Hunt (1969a) developed a numerical method to solve radiative transfer equation in inhomogeneous media. In a subsequent paper (1969b), they also formulated simple conditions for their procedure to be stable and also give non-negative solution. This technique provides us with efficient means for computing internal and emergent radiant intensity in the presence or in the absence of internal radiation sources. Our familiarity with this method and the

flexibility it provides us to include quite a number of physical processes are the reasons to use this method to handle the problems considered in this work.

1.3 Description of the problems in this study

Our study pertains to certain effects of partial redistribution functions on resonance lines and also the effect of small macroscopic velocity fields on Ca II H and K lines. The problems considered in this work are described below in some detail.

Arthur Schuster (1905) proposed the scattering of radiation to be a viable mechanism in the formation of spectral lines in stellar atmospheres.

Radiation field becomes nonlocal due to the scattering process and this sets the nonlocal thermodynamic equilibrium (Non LTE) condition in stellar atmosphere. The coupling of radiation field and the number density of different atomic states is another aspect of Non LTE. Thomas (1965) proved the existence of Non LTE in the outer parts of the stellar atmosphere. We have used the Non LTE theory to study the transfer of line radiation.

In earlier works on line transfer, scattering was assumed to be strictly coherent in the observer's frame of reference (Milne, 1928). In stellar atmospheres, the Doppler redistribution in frequency produced by the thermal motion of

the atoms has to be taken into account. The above process combined with the assumption that there is no correlation between the frequencies of the absorbed and emitted photons, make them completely redistributed (CRD) over the spectral line. Neither of these two extreme situations is achieved in stellar atmospheres and so one has to consider the redistribution of photons in frequency in some detail. This is known as partial redistribution (PRD) mechanism in the literature.

In the process of scattering, an atom is excited from one bound level to another by the absorption of a photon, and decays radiatively back to the original state with the emission of a photon. Different laboratory frame redistribution (LFR) functions exist for describing the line scattering under different conditions. They are denoted as R_I , R_{II} , and R_{III} in Hummer's (1962) notation. The influence of R_I and R_{II} redistribution functions on source functions in semi-infinite and finite isothermal atmospheres was studied by Hummer (1969). Large differences were found to exist in the wings of the lines between the CRD and PRD mechanisms. The role of R_I , R_{II} and R_{III} functions in finite and semi-infinite media were studied by Vardavas (1976 a,b,c). By taking elaborate atomic and atmospheric models, and a combination of R_I and R_{III} functions to describe the redistribution, Shine, Milkey and Mihalas (1975) explained many of the observational aspects of solar Ca II H and K line profiles. Basri (1979) found the PRD mechanism to influence the emission

reversal of Mg II k line. Heinzel (1981) derived the LFR which describes the scattering of radiation when both the atomic levels are radiatively broadened and denoted it as $R_{\mathbf{V}}$. This function is moderately coherent in the wings and so it serves as an intermediate case between highly coherent $R_{\mathbf{II}}$ and non-coherent $R_{\mathbf{III}}$ functions.

Since there is a revival of interest in these partial redistribution functions, we have considered some schematic line formation problems which provide us some useful information about the redistribution of photons in spectral lines. In the second chapter of this thesis we have discussed the effect of $R_{\mathbf{I}}$, $R_{\mathbf{II}}$, $R_{\mathbf{III}}$ and $R_{\mathbf{V}}$ functions on line formation. We have compared these results with those obtained using CRD. We have considered various types of scattering media and boundary conditions.

Chandrasekhar (1948) drew attention to the possibility of broadening of lines by electron scattering. Even though the electron scattering is non-coherent in stellar atmospheric conditions, most of the calculations so far assume that it is coherent. Auer and Mihalas (1968) studied both coherent and non-coherent electron scattering with complete redistribution by atoms. We have extended this work to include partial redistribution by atoms. So in the third chapter, coherent and non-coherent electron scattering combined with complete and partial redistribution by atoms are studied for some parametrized models so that the underlying physical processes

can be understood.

The emission profile ψ_ν is defined as the fraction of all atoms in the upper state that if they decay radiatively, emit photons of frequency ν as seen in the laboratory frame. If the absorption and emission are regarded as two independent processes (CRD situation), the equality of absorption and emission profiles is assured. If there is any correlation between absorption and the subsequent emission, then the emission profile is dependent on the radiation field, and the two profiles need not be identical (Oxenius, 1965). Sub-state formalism of Milkey and Mihalas (1973) enables a quantitative study of this problem. Stenitz and Shine (1973) investigated the assumption of equality of absorption and emission profiles for a two level atom with Doppler redistribution. Baschek, Mihalas and Oxenius (1981) showed that the formulation given by Mihalas (1978) of the stimulated emission term is incorrect. They gave the correct expression for the statistical equilibrium equations for the angle averaged isotropic redistribution function. We have used their expression for the source function to study the deviation of absorption and emission profiles for various redistribution functions. We have used the iteration technique to solve the emission profile and the radiation field.

Asymmetric profiles with a single peak emission of the Ca II K line were observed at high spatial resolution studies of sun (Pasachoff, 1970). To account for the asymmetric

profiles, Athay (1970) assumed velocity fields in the regions of line formation. He concluded that to obtain the K_{2v} enhancement, either the layers where K_2 is formed are moving upward with velocities of 3-7 kms^{-1} or the K_3 layers are moving downward with velocities of 10-20 kms^{-1} . Line formation in moving media was studied by Kulander (1968), Kalkofen (1970) and several other workers. Peraiah (1978) gave an algorithm for solving transfer equation including velocity fields in spherically symmetric expanding media. This program can also be used to study plane parallel geometry with very few changes. We have used this code with the necessary modifications to study the effect of velocities on Ca II H and K lines. We have chosen 5 level atom with continuum as our atomic model and a chromospheric type of temperature rise is assumed. We have solved the coupled transfer and statistical equilibrium equations. There are several methods to solve multi level equations. One of the well known methods is the equivalent two level atom (ETLA) method. This was employed by Linsky and Avrett (1970) to study the formation of Ca II H and K lines in the quiescent Solar atmosphere. A more powerful method is the linearization technique of Auer and Mihalas (1969). Integral equation approach was extended to include the linearization technique by Kalkofen (1974). We have used the ETLA which allows an easy treatment of small macroscopic velocities and also the specific intensity can be directly obtained.

CHAPTER 2

THE EFFECT OF PARTIAL FREQUENCY REDISTRIBUTION

FUNCTION R_I , R_{II} , R_{III} , AND R_V ON THE SPECTRAL

LINE FORMATION

2.1 Introduction

In the earliest analyses of spectral lines, it was assumed that the scattering of photons by atoms is coherent. In stellar atmospheres, the spectral line is produced by an ensemble of atoms with a thermal velocity distribution. Therefore, it is necessary to take into account the Doppler redistribution in frequency produced by the random motion of the atoms. By taking into account the Doppler redistribution and also assuming that there is no correlation between the frequencies of the absorbed and emitted photons, one sees that the photons are completely redistributed over the spectral line. This is better than the coherent scattering assumption. However, to account for the correct description of the frequency redistribution, one has to consider the correlation between the absorbed and emitted frequencies of photon. Unno (1952) derived such a redistribution function, for the case when both the atomic levels between which the

transition occurs, have zero natural width. Henyey (1941) obtained a redistribution function which describes the scattering when the upper level is radiatively broadened. Radiation and collision damping with complete redistribution in the atom's frame combined with thermal Doppler broadening gives a redistribution denoted by R_{III} . The function R_{III} and the other redistribution functions were studied by Hummer (1962). In his notation, Unno's function was denoted as R_{I} and Henyey's as R_{II} .

Source functions become frequency dependent when the redistribution functions are used in the radiative transfer calculations. Such frequency dependent source functions are studied by Hummer (1969) in semi-infinite and finite isothermal atmospheres. In the wings, large differences were found to exist between the complete redistribution (CRD) and partial redistribution (PRD) source functions. The effects of photon frequency and angular redistribution on line formation using R_{I} , R_{II} and R_{III} functions and their role in finite and semi-infinite plane parallel media were studied by Vardavas (1976 a,b,c). He made a comparison of the above results with CRD and also with the results of angle averaged redistribution functions. The differences between the emergent intensity profiles using CRD with a Voigt absorption profile and R_{III} function was found to be negligible (Vardavas, 1976b). Similar conclusion was arrived at by Finn (1967). R_{II} redistribution function which is strongly coherent in the wings was shown to lower the line profile outside the Doppler core. (Hummer, 1969; Vardavas, 1976c). Angle dependent and angle

averaged R_I redistribution functions were studied in spherically symmetric expanding media by Peraiah (1978). In moving media, he obtained P Cygni type of profiles. Milkey and Mihalas (1973) used a combination of R_{II} and R_{III} redistribution functions in explaining solar Lyman- α resonance line profile.

As far as subordinate lines are concerned, Heinzel (1981) derived the correct laboratory frame redistribution function (LFR) for the scattering of radiation assuming both the atomic levels are radiatively broadened. This LFR denoted as R_V is based on Quantum mechanical results of Omont Smith and Cooper (1972). R_V can be applied to low density media like chromospheres, gaseous nebula etc where collisions are few. In a subsequent paper, Heinzel and Hubeny (1982) extended the LFR of Heinzel (1981) to include collisional broadening of both the levels. Some transfer effects of R_V have been discussed by Hubeny and Heinzel (1984). Mohan Rao, Rangarajan and Peraiah (1984) discussed the effects of partial redistribution functions R_I , R_{II} and R_{III} on source functions.

The above work has been extended in this chapter to include optical depth effects and also the R_I redistribution function. Comparison of these results with those obtained using CRD with Doppler and Voigt absorption profiles is made here. Various types of scattering media are considered. The effect of different boundary conditions on the emergent intensity profiles is also studied here. In 2.2 we describe briefly the various redistribution functions employed in this

work. Basic equations and computational procedure are given in 2.3. Discussion of the results is made in 2.4.

2.2 Redistribution functions

2.2.1 Atomic frame redistribution functions

The absorption profile in the atomic frame is given by, say, $f(\xi')$ where ξ' is the frequency of the incoming photon. $p(\xi', \xi)$ gives the probability that a photon absorbed in the frequency range $(\xi', \xi' + d\xi')$ is emitted into the range $(\xi, \xi + d\xi)$ while the angular phase function $g(\mathbf{n}', \mathbf{n})$ describes the probability that a photon is scattered from solid angle $d\omega'$ in direction \mathbf{n}' into solid angle $d\omega$ in direction \mathbf{n} . All these functions are normalized to unity. The joint probability that a photon (ξ', \mathbf{n}') is absorbed and a photon (ξ, \mathbf{n}) is emitted is known as the atomic frame redistribution $r(\xi', \xi)$ (Hummer, 1962).

$$r(\xi', \xi) d\xi' d\xi = \int \int f(\xi') d\xi' p(\xi', \xi) d\xi' \frac{d\omega'}{4\pi} \frac{d\omega}{4\pi} \quad (2.1)$$

If we consider a two level atom (see figure 1) with both levels perfectly sharp, then the absorption and emission can take place at only the line centre frequency ξ_0 . Therefore the absorption profile is given by Dirac delta function :

$$f(\xi') d\xi' = \delta(\xi' - \xi_0) d\xi' \quad (2.2a)$$

Since the emission takes place at the same frequency, the emission probability is

$$p(\xi', \xi) d\xi = \delta(\xi' - \xi) d\xi \quad (2.2b)$$

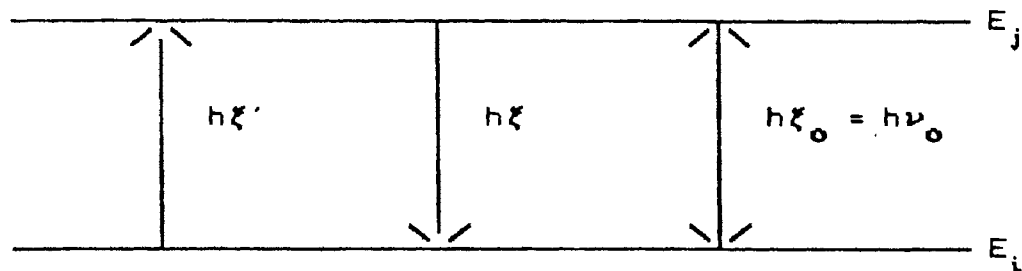


Fig. 1 i and j are the lower and upper states. ξ' , ξ and ξ_0 are the absorption, emission and line centre frequencies measured in atom's frame. h is the Planck constant. Line centre frequency $\xi_0 = \nu_0$ where ν_0 is laboratory frame frequency.

Let us suppose that the upper state is radiatively broadened. Then the absorption profile is described by the Lorentz profile,

$$f(\xi') d\xi' = \frac{\delta d\xi'}{\pi [(\xi' - \xi_0)^2 + \delta^2]} \quad (2.3a)$$

where $\delta = \Gamma_{\mathbf{R}} / 4\pi$ and $\Gamma_{\mathbf{R}}$ is the radiative damping width of the upper state.

Since we have not considered any collisional reshuffling of electrons in the upper state in this case, we find that the emission probability is again given by the Dirac delta function.

$$p(\xi', \xi) d\xi = \delta(\xi' - \xi) d\xi \quad (2.3b)$$

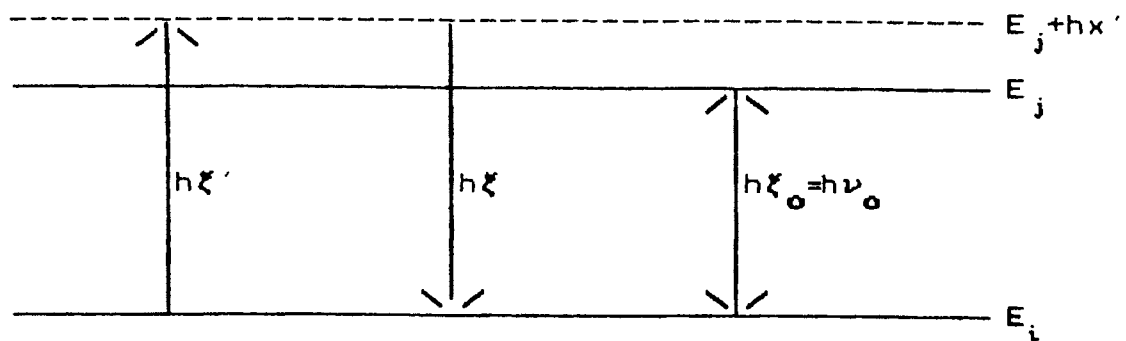


Fig 2. Same as Fig. 1 with upper state radiatively broadened.

In the next case, let us envision an atom with two states and the upper state is broadened by collisions also. The absorption profile is given by

$$f(\xi') d\xi' = \frac{\delta d\xi'}{\pi [(\xi' - \xi_0)^2 + \delta^2]} \quad (2.4a)$$

Now δ denotes the combined width of collisions and radiation (see Fig. 3)

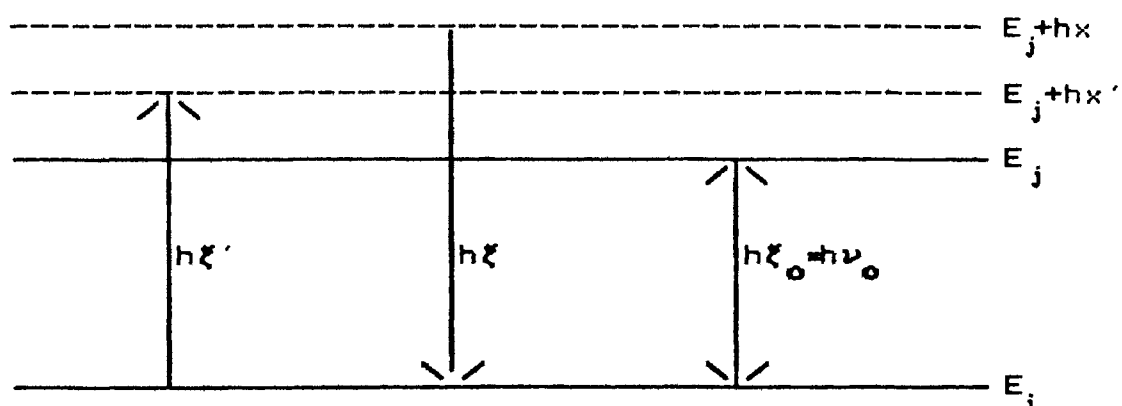


Fig. 3 Same as Fig. 2 but the upper level is broadened collisionally in addition.

In this situation, the frequency of the emitted photon will have no correlation with that of the absorbed photon. The probability of emission at any particular frequency is then proportional to the number of atoms which are capable of emitting at that frequency and hence to the absorption profile itself. Therefore we have

$$p(\xi', \xi) d\xi = f(\xi') d\xi' = \frac{\delta d\xi'}{\pi [(\xi_0 - \xi')^2 + \delta^2]} \quad (2.4b)$$

Now let us go to a more general situation i.e. both the states are radiatively broadened.

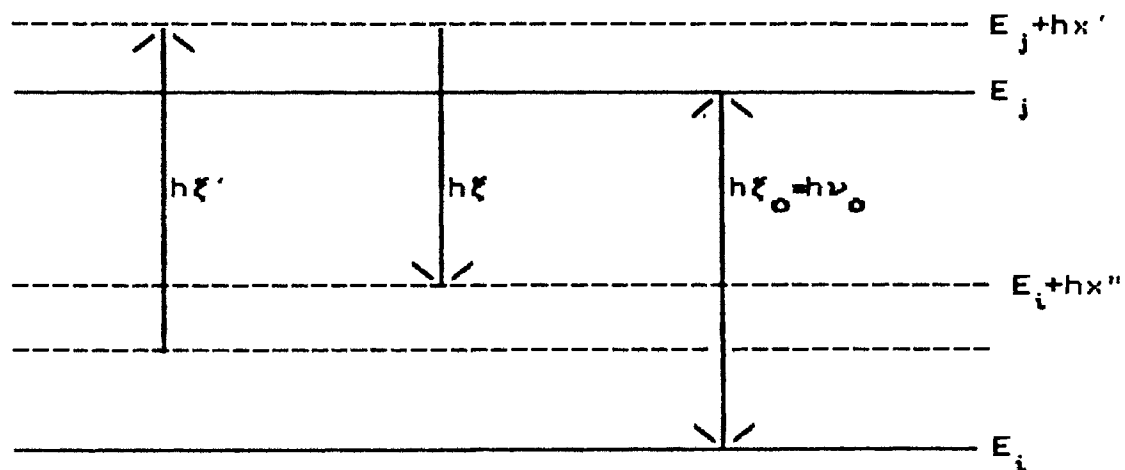


Fig. 4 The states i and j are radiatively broadened. Other symbols have their usual meaning.

Woolley and Stibbs (1953) showed that the atomic frame redistribution in such cases is given by

$$\begin{aligned}
r_{\nu}(\xi, \xi') &= \frac{\delta_i^2 \delta_j}{\pi^2} \frac{1}{[(\xi - \xi')^2 + 4\delta_i^2]} \frac{4(2\delta_i + \delta_j)}{[(\xi' - \nu_0)^2 + (\delta_i + \delta_j)^2][(\xi - \nu_0)^2 + (\delta_i + \delta_j)^2]} \\
&+ \frac{\delta_i \delta_j}{\pi^2} \frac{1}{[(\xi - \nu_0)^2 + (\delta_i + \delta_j)^2][(\xi - \xi')^2 + 4\delta_i^2]} \\
&+ \frac{\delta_i \delta_j}{\pi^2} \frac{1}{[(\xi - \xi')^2 + 4\delta_i^2][(\xi - \nu_0)^2 + (\delta_i + \delta_j)^2]} \\
&+ \frac{\delta_i^2}{\pi^2} \frac{1}{[(\xi' - \nu_0)^2 + (\delta_i + \delta_j)^2][(\xi - \nu_0)^2 + (\delta_i + \delta_j)^2]}
\end{aligned} \tag{2.5}$$

δ_i , δ_j are the damping parameters for the lower and upper states respectively.

2.2.2 Laboratory frame redistribution functions

To obtain the laboratory frame redistribution functions which describe the scattering of photons by atoms in a detailed way one has to consider the Doppler shift introduced by the thermal motion of atoms in addition to the atomic frame redistribution functions mentioned above. Since the Doppler shift depends on the velocity distribution of atoms, Maxwellian velocity distribution is generally employed. To find the net result for the entire ensemble of atoms, we must average over the velocity distribution. The derivations for the first three cases mentioned above are given by Hummer (1962). For the case of r_{ν} , Heinzl (1981) has derived the laboratory frame redistribution function.

Here we sketch briefly the steps required to derive the angle averaged laboratory frame redistribution functions. A detailed description is given in 'Stellar atmospheres' by Mihalas (1978).

Suppose an atom moving with a velocity \mathbf{v} , which remains fixed during the scattering process, absorbs a photon (ν', \mathbf{n}') and emits a photon (ν, \mathbf{n}) as measured in the laboratory frame. Neglecting the aberration of directions in transforming from the atom's frame to the laboratory frame, the corresponding atom's frame frequencies for the absorption and emission are

$$\xi' = \nu' - \nu_0 (\mathbf{v} \cdot \mathbf{n}') / c \quad (2.6a)$$

and
$$\xi = \nu - \nu_0 (\mathbf{v} \cdot \mathbf{n}) / c \quad (2.6b)$$

Then, the joint probability of absorption of a photon (ξ', \mathbf{n}') with subsequent emission of a photon (ξ, \mathbf{n}) measured in the atom's frame is $f(\xi') p(\xi', \xi) g(\mathbf{n}', \mathbf{n}) d\xi' d\xi (d\omega' / 4\pi) (d\omega / 4\pi)$. Transforming this expression to the laboratory frame via equations (2.6 a,b) we can write

$$R(\nu', \mathbf{n}'; \nu, \mathbf{n}) = f(\nu' - \nu_0 \mathbf{v} \cdot \mathbf{n}' / c) p(\nu' - \nu_0 \mathbf{v} \cdot \mathbf{n}' / c, \nu - \nu_0 \mathbf{v} \cdot \mathbf{n} / c) g(\mathbf{n}', \mathbf{n}) \quad (2.7)$$

For convenience, expressing velocities in dimensionless thermal units

$$\mathbf{u} = \mathbf{v} / v_{\text{thermal}} = (m_{\text{A}} / 2kT)^{1/2} \mathbf{v} \quad (2.8)$$

where m_{A} is the mass of an atom. Let us introduce the Doppler width

$$w = (\nu_0 / c) (2kT / m_{\text{A}})^{1/2} = \nu_0 (v_{\text{thermal}} / c) \quad (2.9)$$

Rewriting equation (2.7) using the Doppler units defined in equations (2.8) and (2.9):

$$R(\nu', \mathbf{n}'; \nu, \mathbf{n}) = f(\nu' - w\mathbf{u} \cdot \mathbf{n}') p(\nu' - w\mathbf{u} \cdot \mathbf{n}', \nu - w\mathbf{u} \cdot \mathbf{n}) g(\mathbf{n}', \mathbf{n}) \quad (2.10)$$

Choose an orthonormal triad $(\mathbf{n}_1, \mathbf{n}_2, \mathbf{n}_3)$ such that $\mathbf{u} = u\mathbf{n}_3$. Then $\mathbf{u} \cdot \mathbf{n} = \mu$ and $\mathbf{u} \cdot \mathbf{n}' = \mu'$, where $\mu = \mathbf{n} \cdot \mathbf{n}_3$ and $\mu' = \mathbf{n}' \cdot \mathbf{n}_3$. An element of solid angle may be written $d\omega = d\mu d\phi$ where ϕ is the azimuthal angle around \mathbf{n}_3 . The phase function $g(\mathbf{n}', \mathbf{n})$ can be expressed in general as $g(\mu', \mu, \phi)$. Thus angle averaging equation (2.10) we have

$$R(\nu', \nu) = (16\pi^2)^{-1} \int_0^{2\pi} d\phi \int_{-1}^1 d\mu' f(\nu' - w\mu' u) \int_0^{2\pi} d\phi' g(\mu', \mu, \phi') \times \int_{-1}^1 d\mu p(\nu' - w\mu' u, \nu - w\mu u) \quad (2.11)$$

$$\text{Defining } g(\mu', \mu) \equiv (4\pi)^{-1} \int_0^{2\pi} g(\mu', \mu, \phi') d\phi' \quad (2.12)$$

we get

$$R_u(\nu', \nu) = \frac{1}{2} \int_{-1}^1 d\mu' f(\nu' - w\mu' u) \int_{-1}^1 d\mu g(\mu', \mu) p(\nu' - w\mu' u, \nu - w\mu u) \quad (2.13)$$

For isotropic scattering $g(\mu', \mu) \equiv \frac{1}{2}$. Employing this result in the above equation we get,

$$R_u(\nu', \nu) = \frac{1}{4} \int_{-1}^1 d\mu' f(\nu' - w\mu' u) \int_{-1}^1 d\mu p(\nu' - w\mu' u, \nu - w\mu u) \quad (2.14)$$

If the scattering is coherent in the atomic frame,

$$p(\nu' - w\mu' u, \nu - w\mu u) = \delta[\nu' - \nu - wu(\mu' - \mu)] \quad (2.15)$$

Because the range of integration for μ' and μ is only $(-1, 1)$, it is clear that for a given value of u , the singularity of the δ -function will be outside the range of

integration for sufficiently large values of $|\nu' - \nu|$ and $R_u(\nu', \nu)$ will, accordingly, be zero. Physically this corresponds to the fact that an atom moving with velocity u can change a photon's frequency by no more than $2uw$, this maximum shift occurring if the propagation vectors of the incoming and outgoing photons lie along the velocity vector and are oppositely directed. Let $y \equiv w\mu u$, and write

$$I = (wu)^{-1} \int_{-wu}^{wu} \delta \left[y - (\nu - \nu' + w\mu' u) \right] dy \quad (2.16)$$

The integral will equal $(1/wu)$ if $-wu \leq \nu - \nu' + w\mu' u \leq wu$, and will be zero otherwise. Define $\Lambda(x)$ such that $\Lambda = 1$ if $-1 \leq x \leq 1$, and $\Lambda = 0$ otherwise. Then equation (2.14) can be rewritten using equation (2.16) as

$$R_u(\nu', \nu) = (4wu)^{-1} \int_{-1}^1 f(\nu' - w\mu' u) \Lambda \left[\mu' + (wu)^{-1} (\nu - \nu') \right] d\mu' \quad (2.17)$$

If u is sufficiently small, then $|(\nu - \nu')/wu| \geq 1$ and Λ will vanish for all values of μ' . Thus there is a minimum speed u_{\min} , for which scattering from ν' to ν can occur. Define $\bar{\nu} \equiv \max(\nu', \nu)$ and $\underline{\nu} \equiv \min(\nu', \nu)$. The requirement that the argument of the Λ -function fall in the range $(-1, 1)$ yields

$$u_{\min} = (\bar{\nu} - \underline{\nu})/2w = |\nu - \nu'|/2w \quad (2.18)$$

For $u < u_{\min}$, R_u will be zero. For $u > u_{\min}$, a contribution to R_u will come from part of the range of integration over μ' .

$$-1 \leq \mu' \leq 1 - \left[(\bar{\nu} - \underline{\nu})/wu \right]$$

Now introducing the *Heaviside function* $\mathbb{H}(x, x_0)$, defined such

that $\Phi = 1$ when $x > x_0$ and 0 otherwise and also substituting $y \equiv \nu' - wu$ in equation (2.17) we get

$$R_u(\nu', \nu) = (4w^2 u^2)^{-1} \Phi(u - |\nu - \nu'|/2w, 0) \int_{\nu - wu}^{\nu + wu} f(y) dy \quad (2.19)$$

Finally averaging over the Maxwellian velocity distribution

$$P(u) du = \pi^{-3/2} e^{-u^2} (4\pi u^2) du \quad (2.20)$$

we get the following expression for coherence in the atom's frame (cases I and II as described below)

$$R(\nu', \nu) = (\pi^{1/2} w^2)^{-1} \int_{u_{\min}}^{\infty} du e^{-u^2} \int_{\nu - wu}^{\nu + wu} f(y) dy \quad (2.21)$$

Transforming $R_A(\nu', \nu)$ to Doppler units,

$$\begin{aligned} x' &= (\nu' - \nu_0)/w ; & x &= (\nu - \nu_0)/w \\ R(x', x) &= w^2 R(\nu', \nu) (d\nu'/dx') (d\nu/dx) \end{aligned} \quad (2.22)$$

RESULTS FOR SPECIFIC CASES

(a) Case I: This corresponds to the scattering of a photon by an atom with two perfectly sharp states and so $f(y) = \delta(y - \nu_0)$; u_{\min} now becomes effectively $u'_{\min} = \max(|x'|, |x|)$. Then from equations (2.21) and (2.22)

$$R_I(x, x) = \pi^{-1/2} \int_{u_{\min}}^{\infty} e^{-u^2} du = \frac{1}{2} \operatorname{erfc}(u'_{\min}) \quad (2.23)$$

where the complimentary error function is defined as

$$\operatorname{erfc}(x) = 2\pi^{-1/2} \int_x^{\infty} e^{-z^2} dz \quad (2.23a)$$

Substituting for u'_{\min} ,

$$R_I(x', x) = \frac{1}{2} \operatorname{erfc} \left[\max(|x|, |x'|) \right] \quad (2.24)$$

The profile of absorption function is given by,

$$\phi(x') = \int_{-\infty}^{\infty} R(x', x) dx \quad (2.25)$$

$\phi(x)$ can also be derived from first principles. Thus considering the equations (2.14) and (2.20)

$$\phi(\nu') = \frac{1}{\sqrt{\pi}} \int_0^{\infty} u^2 e^{-u^2} du \int_{-1}^1 f(\nu' - w\mu'u) d\mu' \int_{-1}^1 \int_0^{\infty} P(\nu' - w\mu'u; \nu - w\mu u) d\nu d\mu \quad (2.26)$$

Since P is the emission probability, the inner integral over ν in the above equation gives unity and the integral over μ , a factor of 2. Therefore the above equation reduces to,

$$\phi(\nu') = \frac{2}{\sqrt{\pi}} \int_0^{\infty} u^2 e^{-u^2} du \int_{-1}^1 f(\nu' - w\mu'u) d\mu' \quad (2.27)$$

For case I, $f(y) = \delta(y - \nu_0)$. Therefore equation (2.27) becomes,

$$\phi(\nu') = \frac{2}{\sqrt{\pi}} \int_0^{\infty} u^2 e^{-u^2} du \int_{-1}^1 \delta(\nu' - \nu_0 - w\mu'u) d\mu' \quad (2.28)$$

The integral over μ' exists only when $u_{\min} \geq |(\nu' - \nu_0)/w|$ and is

equal to $1/wu$. Thus we get after transforming to Doppler units

$$\phi(x') = \frac{1}{\sqrt{\pi}} \int_{x'}^{\infty} 2u e^{-u^2} du = \frac{1}{\sqrt{\pi}} e^{-x'^2} \quad (2.29)$$

The complimentary error function in equation (2.23a) is evaluated using the Rational approximation method given in 'Mathematical functions' by Abramovitz and Stegun (1974). This R_I function describes an idealized situation. Normally one of the atomic states will be broadened. Still it is useful to study this limiting case, for, it demonstrates the effects of Doppler redistribution alone as seen by an observer in the laboratory frame examining an ensemble of moving atoms. $R_I(x', x)/\phi(x')$ which is plotted in Fig 5(a) is the probability of emission at frequency x per absorption when the absorption is at x' . This is in good agreement with that given in Mihalas (1978).

We see from Figure 5(a) that a photon absorbed at frequency x' is emitted with equal probability at all x such that $-|x'| \leq |x| \leq |x'|$ and with exponentially decreasing probability beyond this range. In the atom's frame, absorption and emission occur at only the line centre frequency. Therefore if an atom is absorbing at frequency x' means that it is moving with a velocity of x' Doppler units. The photon which is absorbed has an equal probability of being emitted in all directions because of isotropic phase function. Therefore it has equal probability of being emitted in the above range.

(b) Case II: Here the lower level is sharp and the upper level is radiatively broadened. The absorption profile in the atom's frame is given by the expression (2.3a). Transforming it to laboratory frame and substituting that expression in equation (2.21) we get,

$$R_{II}(\nu', \nu) = (w^2 \pi^{3/2})^{-1} \delta \int_{u_{\min}}^{\infty} du e^{-u^2} \int_{\bar{\nu}-wu}^{\nu+wu} dy [(y-\nu_0)^2 + \delta^2]^{-1}$$

converting to Doppler units we have

$$R_{II}(x', x) = \frac{1}{\pi^{3/2}} \int_{|x'-x|/2}^{\infty} e^{-u^2} \left[\tan^{-1} \left[\frac{x+u}{a_j} \right] - \tan^{-1} \left[\frac{\bar{x}-u}{a_j} \right] \right] du \quad (2.30)$$

where $\bar{x} \equiv \max(|x|, |x'|)$ and $\underline{x} \equiv \min(|x|, |x'|)$ and $a_j = \delta/w$, is the damping constant for upper level. A typical value of 2×10^{-3} for a_j is chosen.

DERIVATION OF PROFILE FUNCTION

Now the absorption coefficient in the atomic frame is given by equation (2.3a). Substituting that after suitable transformations in equation (2.27) we get,

$$\phi(\nu') = \frac{2\delta}{\pi^{3/2}} \int_0^{\infty} u^2 e^{-u^2} du \int_{-1}^1 \frac{1}{(\nu' - \nu_0 - w\mu'u)^2 + \delta^2} d\mu' \quad (2.31)$$

Substituting $y = \nu' - w\mu'u$ in the above equation we get,

$$\phi(\nu') = \frac{2\delta}{w\pi^{3/2}} \int_0^{\infty} u e^{-u^2} du \int_{\nu'-wu}^{\nu'+wu} \frac{1}{(y-\nu_0)^2 + \delta^2} dy$$

Converting to Doppler units and integrating over y we get,

$$\phi(x') = \frac{a_j}{\pi^{3/2}} \int_0^{\infty} d(e^{-u^2}) \left[\tan^{-1} \left[\frac{x'+u}{a_j} \right] - \tan^{-1} \left[\frac{x'-u}{a_j} \right] \right]$$

Integrating the above equation by parts we get,

$$\phi(x') = \frac{a_j}{\pi^{3/2}} \int_{-\infty}^{\infty} \frac{e^{-u^2} du}{(x'-u)^2 + a_j^2} = H(a_j, x') \quad (2.32)$$

where H is the Voigt function. This scattering process applies to resonance lines in low density media where collisional broadening of upper level is negligible like that of Hydrogen Lyman - α in the interstellar medium. From the plot of $R_{II}(x', x) / \phi(x')$ in fig 5(b) we see the coherency for the wing photons and also that they have the least probability of being emitted at the line centre. In Doppler core, R_{II} behaves like other redistribution functions. Most of the atoms will be moving with low velocities and they absorb near the line centre. Once they absorb near line centre, they are going to emit in the Doppler core according to the mechanism described for R_I function. Absorption in the atom's frame follows a Lorentzian distribution which allows the photons to be absorbed in the wings away from the line centre. Since the emission process is coherent, the emission also takes place in the line wing. Emitted frequency is not doppler shifted because of the low velocities involved. Therefore we see in the line core, there is Doppler redistribution and strong non-coherence, while in the wing the scattering is more nearly coherent for R_{II} . Fig 5(b) is in complete agreement with that of Heinzel and Hubeny (1983).

Case III: Here we consider the collisional broadening of the upper level. Substituting the forms for absorption and emission coefficients from equations (2.4a) and (2.4b) in equation (2.14) and making the appropriate transformations, we get,

$$R_{\text{III}}(\nu', \nu) = \frac{1}{4} \int_{-1}^1 \frac{(\delta/\pi) d\mu'}{(\nu' - w\mu'u - \nu_0)^2 + \delta^2} \int_{-1}^1 \frac{(\delta/\pi) d\mu}{(\nu - w\mu - \nu_0)^2 + \delta^2}$$

Averaging over a Maxwellian velocity distribution and converting to Doppler units we have

$$R_{\text{III}}(x', x) = \pi^{-\frac{5}{2}} \int_0^{\infty} e^{-u^2} \left[\tan^{-1} \left[\frac{x' + u}{a_j} \right] - \tan^{-1} \left[\frac{x' - u}{a_j} \right] \right] \\ \times \left[\tan^{-1} \left[\frac{x + u}{a_j} \right] - \tan^{-1} \left[\frac{x - u}{a_j} \right] \right] du \quad (2.33)$$

Absorption profile is defined in a similar way as in the case of R_{II} . $R_{\text{III}}(x', x)/\phi(x')$ for $a_j = 2 \times 10^{-3}$ and 10^{-3} are plotted in figures 5(c) and 5(d). We see that the wing photons get completely redistributed and they have a high probability of being emitted at the line centre. This is due to the fact that the emission in the atom's frame follows Lorentzian distribution which peaks at line centre frequency. Fig 5(d) is in good agreement with that of Finn (1967).

When the lower and upper levels are broadened by radiative damping, the angle dependent laboratory frame redistribution is given by (Heinzel, 1981),

$$R_{\mathbf{v}}(\mathbf{x}', \mathbf{n}'; \mathbf{x}, \mathbf{n}) = \frac{1}{4\pi^2 \sin \Theta} \left[H \left(\alpha_j \sec \frac{\Theta}{2}, \frac{\mathbf{x} + \mathbf{x}'}{2} \sec \frac{\Theta}{2} \right) \right. \\ \left. \times H \left(\alpha_i \sec \frac{\Theta}{2}, \frac{\mathbf{x} + \mathbf{x}'}{2} \sec \frac{\Theta}{2} \right) + E_{\mathbf{v}}(\mathbf{x}', \mathbf{x}, \Theta) \right] \quad (2.34)$$

where Θ is the angle of scattering. \mathbf{n}' and \mathbf{n} denote the directions of the flight of the absorbed and emitted photons and they satisfy the relation $\cos \Theta = \mathbf{n} \cdot \mathbf{n}'$. The function $E_{\mathbf{v}}$ is given by

$$E_{\mathbf{v}}(\mathbf{x}', \mathbf{x}, \Theta) = \frac{\sin \Theta/2}{\sqrt{\pi}} \operatorname{Re} \int_0^{\infty} e^{-t^2} \left[e^{-2\omega t} + e^{-2\omega' t} \right] \Delta(t) dt \quad (2.35)$$

$$\text{where } \Delta(t) = D(Z + t \cos \Theta/2 + \alpha_i \sec \Theta/2) - D(Z + t \cos \Theta/2) \quad (2.36)$$

$$Z = \sec \Theta/2 \left(\alpha_j - i \frac{\mathbf{x} + \mathbf{x}'}{2} \right) \\ \omega = \alpha_i + \alpha_j - i\mathbf{x} \quad (2.37) \\ \omega' = \alpha_i + \alpha_j - i\mathbf{x}' \\ D(\omega) = H(p, q) + i K(p, q) \quad ; \quad \omega = p - i q$$

$$K(p, q) = \frac{2}{\sqrt{\pi}} \int_0^{\infty} e^{-t^2 - 2pt} \sin(2qt) dt$$

α_i and α_j being the damping constants for lower and upper levels respectively. $\alpha_i = \alpha_j = 10^{-3}$ is chosen for our purposes. The common Voigt functions $H(p, q)$ and $K(p, q)$ are computed using the method due to Matta and Reichel (1971).

Evaluation of E-term

The integral in equation (2.35) can be approximated with a numerical quadrature as (Heinzel, 1981)

$$E_{\nu}(x', x, \Theta) \cong \frac{\sin \Theta/2}{\sqrt{\pi}} \operatorname{Re} \sum_{i=0}^M \int_{t_i}^{t_i+h} e^{-t^2} \left[e^{-2wt} + e^{-2w't} \right] \Delta(t) dt \quad (2.38)$$

where t_0 is 0 and h is the integration step. The complex function $\Delta(t)$ can be expanded as

$$\Delta(t) \cong \Delta(t_i) + \alpha(t-t_i) \Delta_1(t_i) + \frac{\alpha^2}{2} (t-t_i)^2 \Delta_2(t_i) + \dots \quad (2.39)$$

$$\begin{aligned} \text{with } \Delta_1(t_i) &= D_1(Z + \alpha t_i + \alpha' \alpha_i) - D_1(Z + \alpha t_i) \\ \Delta_2(t_i) &= D_2(Z + \alpha t_i + \alpha' \alpha_i) - D_2(Z + \alpha t_i) \\ \alpha &= \cos \Theta/2, \quad \alpha' = \sin \Theta/2 \end{aligned} \quad (2.40)$$

The complex derivatives of $D(u)$ follow the recurrence relations (Heinzel, 1978)

$$\begin{aligned} D_1(u) &= 2u D(u) - 2/\sqrt{\pi} \\ D_2(u) &= 2u D_1(u) + 2D(u) \end{aligned} \quad (2.41)$$

In the above reference (Heinzel, 1981), the terms up to only the first order are given. But to obtain accurate results we find that one has to consider 2nd order terms. Here we are showing explicitly for the first time, the forms of the second order terms. Inserting equation (2.39) into equation (2.38) and relating terms up to second order we obtain

$$\begin{aligned} E_{\nu}(x', x, \Theta) &= \frac{\sin \Theta/2}{\sqrt{\pi}} \operatorname{Re} \sum_{i=0}^M \left\{ \Delta(t_i) \left[\phi_i(w) + \phi_i(w') \right] \right. \\ &\quad \left. + \alpha \Delta_1(t_i) \left[\psi_i(w) + \psi_i(w') \right] + \frac{\alpha^2}{2} \Delta_2(t_i) \left[\eta_i(w) + \eta_i(w') \right] \right\} \end{aligned} \quad (2.42)$$

$$\begin{aligned}\phi_i(w) &= \int_{t_i}^{t_i+h} e^{-t^2-2wt} dt = \frac{\sqrt{\pi}}{2} e^{w^2} \left[\operatorname{erfc}(t_i+w) - \operatorname{erfc}(t_i+w+h) \right] \\ \psi_i(w) &= \int_{t_i}^{t_i+h} e^{-t^2-2wt} (t-t_i) dt \\ &= \frac{e^{w^2}}{2} \left[e^{-(t_i+w)^2} - e^{-(t_i+w+h)^2} \right] - (w+t_i) \phi_i(w)\end{aligned}\quad (2.43)$$

$$\begin{aligned}\eta_i(w) &= \int_{t_i}^{t_i+h} e^{-t^2-2wt} (t-t_i)^2 dt \\ &= \frac{e^{w^2}}{2} \left[e^{-(t_i+w)^2} \frac{1}{(t_i+w)} - e^{-(t_i+w+h)^2} \frac{1}{(t_i+w+h)} \right] \\ &\quad + \frac{\phi_i(w)}{2} - (w+t_i)^2 \phi_i(w) - 2\psi_i(w) (w+t_i)\end{aligned}\quad (2.44)$$

We evaluated ϕ , ψ and η functions in separate modules and substituted the values in the summation (2.42) to obtain the E_v function.

The angle averaged expression can be obtained by

$$R_v(x', x) = 8\pi^2 \int_0^\pi R_v(x', x, \theta) \sin \theta d\theta \quad (2.45)$$

The corresponding absorption profile is

$$\phi(x') = \int_{-\infty}^{\infty} R_v(x', x) dx = H(a_i + a_j, x') \quad (2.46)$$

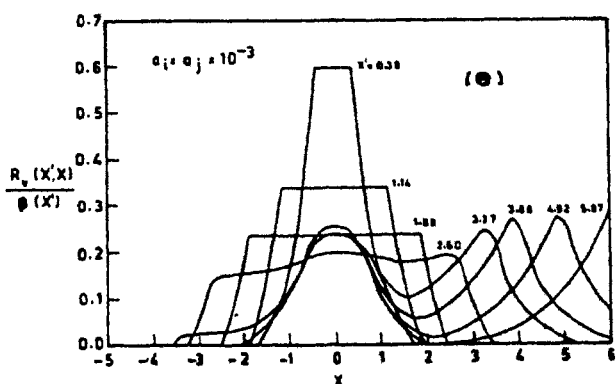
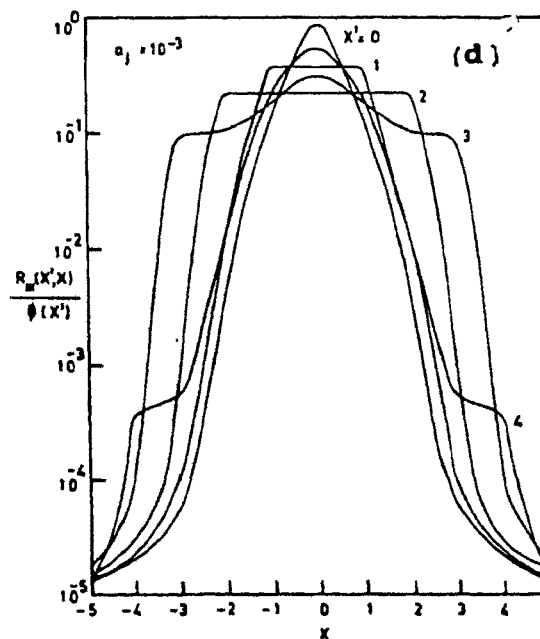
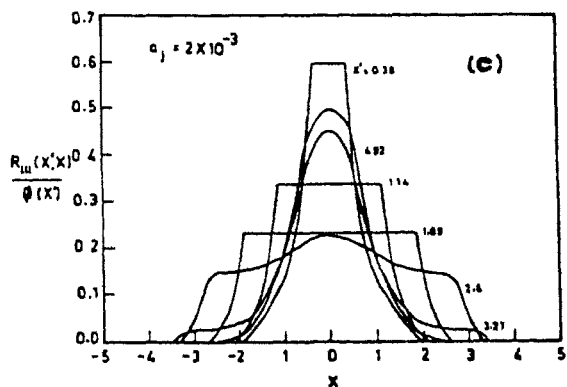
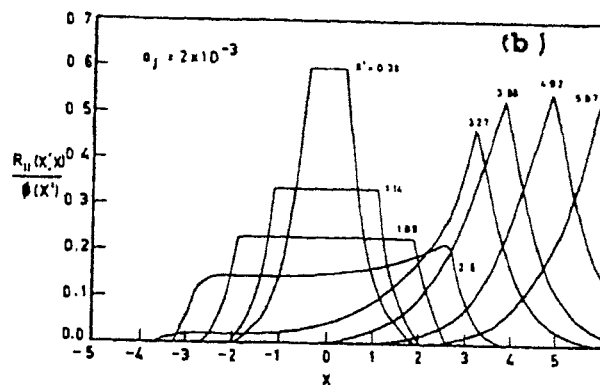
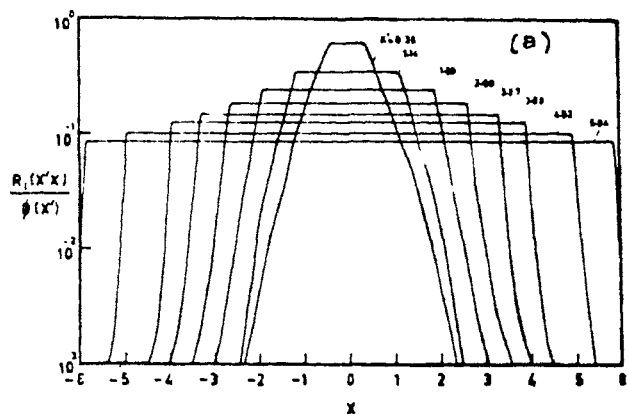


Figure 5. The probability of emission $R(x',x)/\phi(x')$ at frequency x per absorption when the absorption is at frequency x' is plotted for (a) R_I (b) R_{II} with $a_j = 2 \times 10^{-3}$ (c) R_{III} with $a_j = 2 \times 10^{-3}$ (d) R_{IV} with $a_j = 10^{-3}$ (e) R_V with $a_i = a_j = 10^{-3}$.

We employed Gaussian quadrature points with 20 angles to evaluate the integral in equation (2.45). Equation (2.46) can be derived in the same lines as that of equation (2.32).

From the expression for the atomic frame redistribution r_{ν} (eq.2.5) we see that it has maxima at $\xi' = \xi$ and $\xi = \xi_0$. Line centre frequency ξ_0 in atom's frame transforms to ν_0 in laboratory frame, and does not change in magnitude. The underlying physics is discussed by Mihalas (1978). We see that the same trend is reflected in the LFR which can be discerned from fig 5(e). $R_{\nu}(x',x)/\phi(x')$ is plotted in fig 5e. From this figure, we see that a photon when absorbed in the wings, has a high probability of being emitted in the wing as well as at the centre. The wing emission is similar to that of R_{II} function and the emission at the centre resembles that of R_{III} .

2.2.3. Symmetry properties of the LFRs

We see that the equations (2.24), (2.30), (2.33) and (2.34) satisfy the following relations:

$$R_i(-x', -x) = R_i(x', x) \quad ; \quad R_i(x', x) = R_i(x, x') \quad i = I, II, III, V$$

$$R_{I, III}(x', x) = R_{I, III}(x', -x) \quad (2.47)$$

These symmetry relations can be used to advantage while calculating the redistribution functions. Because of them, nearly one fourth of the redistribution matrix elements only need to be computed.

2.3. Basic equations and the computational procedure.

The equation of transfer for a two level atom with plane parallel geometry is given by

$$\mu \frac{dI(x, \mu, z)}{dz} = \kappa_L(z) \left[\beta + \phi(x) \right] \left[S(x, z) - I(x, \mu, z) \right] \quad (2.48)$$

and for the oppositely directed beam

$$-\mu \frac{dI(x, -\mu, z)}{dz} = \kappa_L(z) \left[\beta + \phi(x) \right] \left[S(x, z) - I(x, -\mu, z) \right] \quad (2.49)$$

where $I(x, \mu, z)$ is the specific intensity at angle $\theta = \cos^{-1} \mu$, [$\mu \in (0, 1)$] at the geometrical point z and frequency $x = (\nu - \nu_0)/\Delta\nu$, $\Delta\nu$ being some standard frequency interval. θ is the angle between the ray and the normal to the surface at z . The source function $S(x, z)$ is given by

$$S(x, z) = \frac{\phi(x) S_L(x, z) + \beta S_c}{\phi(x) + \beta} \quad (2.50)$$

where S_L and S_c refer to the source functions in the line and continuum respectively. The line source function is given by

$$S_L(x, z) = \frac{(1-\epsilon)}{2\phi(x)} \int_{-\infty}^{\infty} \int_{-1}^1 R(x', x) I(z, x', \mu') d\mu' dx' + \epsilon B \quad (2.51)$$

where ϵ is the probability per scatter that a photon is destroyed by collisional de-excitation. B is the Planck function. We have set $S_c = B = 1$ in all cases. β is the ratio of continuous opacity per Doppler width to the line opacity.

The above equations are solved within the framework of Discrete space theory technique (Grant and Peraiah, 1972). The

computer code given by Feraiah (1978) is modified to exploit the symmetry properties of the problem and also to include any type of redistribution function with the least number of changes in the program. Gaussian quadrature points are used for frequency and angular mesh. 24 frequency points and two angles are chosen. Since the solution to these equations is symmetric with respect to the line centre, only the positive frequency grid is considered. For evaluation of the scattering integral in equation (2.51) the technique described by Adams, Hummer and Rybicki (1971) is adopted.

2.4 Results and discussion.

2.4.1 Optically thin pure scattering medium ($\epsilon = 0$)

Fig 6 gives the emergent intensity as a function of frequency for a purely scattering atmosphere. The CRD case with Doppler and Voigt absorption profiles (damping parameter $\alpha = 2 \times 10^{-3}$) are also plotted for the purpose of comparison. Boundary conditions considered are:

$$I(x, \mu, \tau = T) = 1 \quad ; \quad I(x, -\mu, \tau = 0) = 0$$

Total optical depth considered is = 155. The criterion for determining whether the medium is effectively optically thick or thin is given by (Hummer, 1965)

$$\epsilon T \gg 1 \quad \text{for Doppler profile.}$$

$$\epsilon(T/\alpha)^{1/2} \gg 1 \quad \text{for Voigt profile.}$$

Since the wings are optically thin, the photons escape in the wings freely and the emergent intensity is nearly the same as the incident intensity. The intensity profiles due to R_I , R_{II} and R_V are nearly the same.

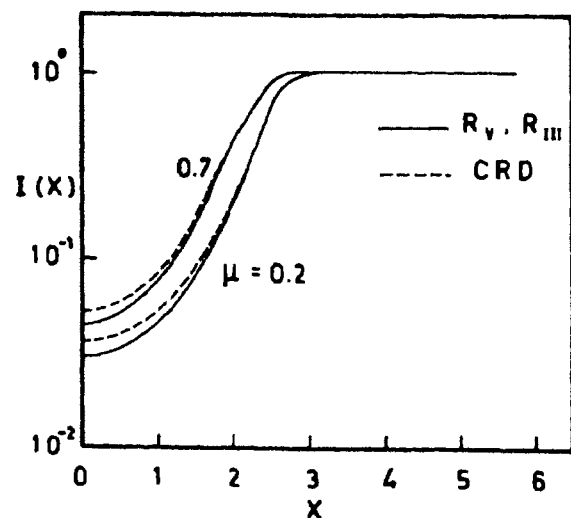


Figure 6 Emergent intensities for R_V and R_{III} are compared with CRD at $\mu = 0.2$ and 0.7 for the case $\epsilon = \beta = 0$ and $T = 155$.

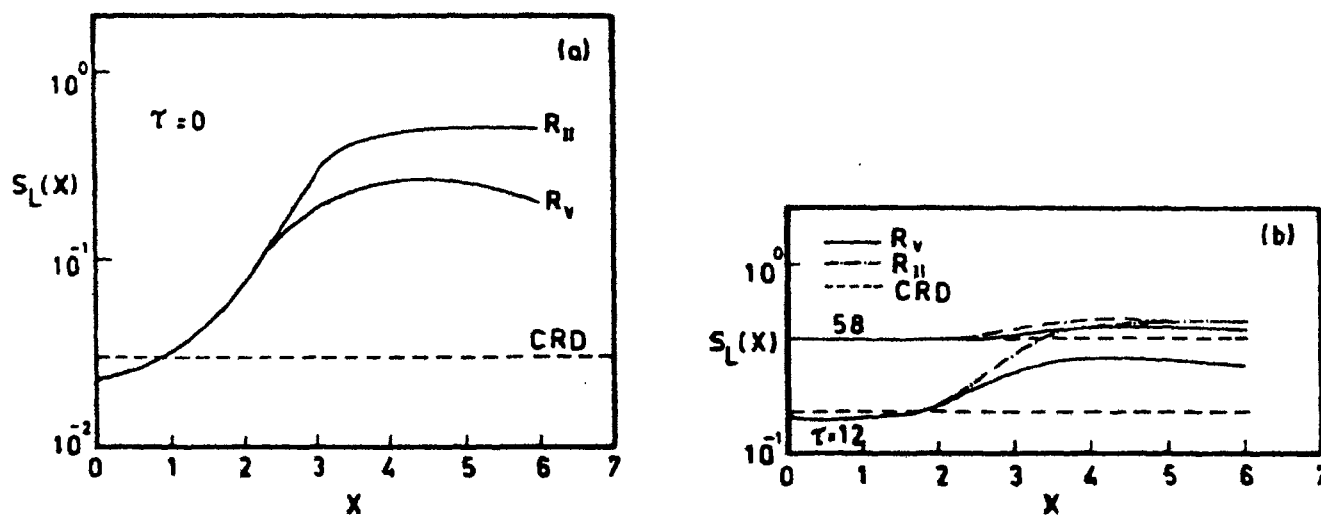


Figure 7 Source functions for R_{II} , R_V and CRD are compared for the case $\epsilon = \beta = 0$, $T = 155$ (a) $T = 0$ (b) $T = 12$ and 58

The source function at various depth points is plotted in fig 7 as a function of frequency. We see that the emergent source function differs from CRD by an order of magnitude in the wings for R_{II} and R_{V} . For a purely scattering medium with small optical depth, there is a substantial contribution to the scattering integral from radiation in the wings. This contribution is enhanced by the fact that R_{II} and R_{V} emergent source functions are higher in the wings compared to CRD. R_{II} source function lies higher than R_{V} since R_{II} is more coherent in the wings as seen from figure 7(a).

Deeper in the medium, the radiation in the wings does not differ very much from the core. This is because the incident radiation has not undergone much of absorption in the core. From figure 7(b) it is clear that the differences between the source function values in the wings are reduced for R_{II} , R_{V} and CRD and also that they do not deviate very much from the values corresponding to the line centre.

2.4.2 Optically thin scattering medium with thermal sources.

When thermal sources ($\epsilon = 10^{-3}$, $B = 1$) are added throughout to the above medium the spectral line becomes shallow with higher intensity at the line centre. The ratio (R) of the intensity due to the pure scattering medium to that of the medium with thermal sources is given by

$$R(x, \mu) = \frac{I(x, \mu, \tau = 0) \text{ pure scattering medium}}{I(x, \mu, \tau = 0) \text{ medium with thermal sources}}$$

Table 1 Ratio R as defined in the text at different frequencies and angles.

$\mu \backslash x$	R(x, μ)						
	0.318	1.12	1.89	2.6	3.27	3.9	3.97
0.21	0.71	0.72	0.78	0.96	0.99	1.00	1.00
0.78	0.72	0.73	0.88	0.99	1.00	1.00	1.00

When analysing the above table one should remember that the medium with thermal sources ($\epsilon \neq 0$) has in addition incident radiation at the lower boundary. From the higher layers where optical depth is low (at line core), we get the radiation from thermal sources. Since the radiation field is unattenuated, we get higher intensity at line core compared to a pure scattering medium where radiation comes from deeper layers and is absorbed giving us a deeper absorption profile. The line wings are optically thin and hence the radiation escapes easily whatever be the sources in the medium. Therefore the wing intensities do not differ for the two different types of media. Both the media do not have continuous source function because we have assumed $\beta = 0$.

2.4.3. Pure scattering medium with high optical depth

when the total optical depth at the line centre is increased to 5×10^4 , the emergent intensity profile at $\mu = 0.78$

for a purely scattering medium is different for different redistribution functions as shown in fig 8. R_I produces deeper profile compared to other functions. This is because R_I has Doppler absorption profile and hence most of the absorption occurs at the line centre while there is less absorption in the wings. Therefore there is no chance for the photons from the wings to be re-emitted at the line centre and this results in less intensity at the core. The same reason makes the wings to be transparent to photons which gives higher intensity in the wings for R_I compared to others. For the other redistribution functions, absorption in the wings does take place because of high optical depth due to the Voigt absorption profile given by these redistribution functions. The high coherency displayed by R_{II} function does not allow the photons to diffuse from the wings to the centre. Therefore the more noncoherent the redistribution is, the higher would be the emergent intensity at the core for a purely scattering medium with high optical depth which can be seen from the above figure. The emergent intensity follows the same behaviour at $\mu = 0.21$.

2.4.4. Optically thick scattering medium with thermal sources.

Thermal emission dominates the picture when thermal sources are added to the above medium. The photons are re-emitted according to Doppler redistribution in the core. Therefore all the redistribution functions give the same intensity in the core. The diffusion of energy takes place from the core to the wing according to the particular type of

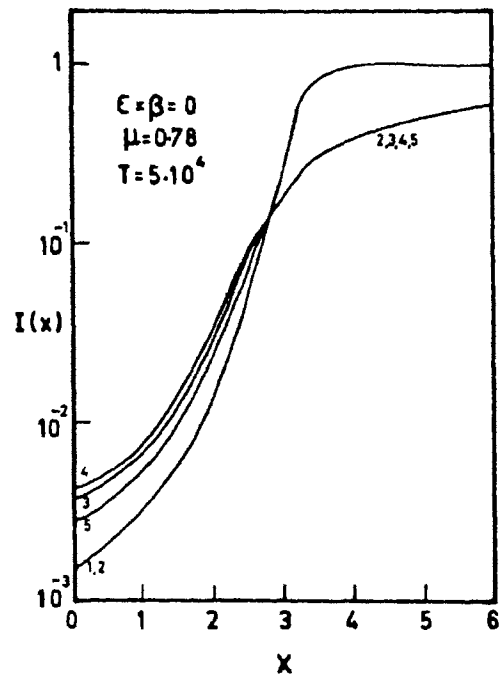


Figure 8 Emergent intensity for the pure scattering medium. ($\epsilon = \beta = 0$). The numbers denote the following cases: (1) R_I (2) R_{II} (3) R_{III} (4) CRD with Voigt absorption profile (VAP) (5) R_V .

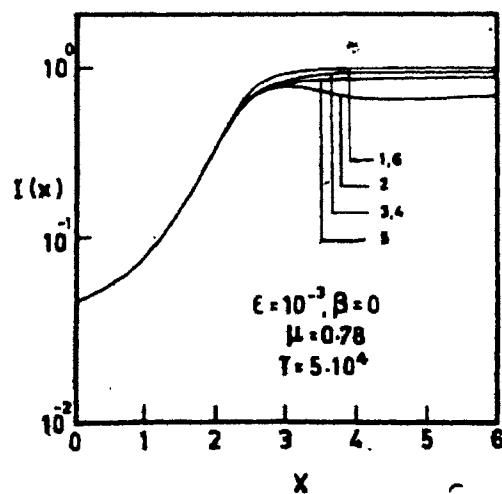


Figure 9 Same as figure 8 for $\epsilon = 10^{-3}$, $\beta = 0$ (6) CRD with Doppler absorption profile

redistribution function. R_{II} does not allow this diffusion easily and so it produces less intensity in the wings. Therefore, for this case also, the more non-coherent the redistribution is, the higher will be the intensity in the wings which can be seen from figure 9.

2.4.5. Medium with only internal sources.

The above result can be illustrated in a more dramatic way if we remove the direct radiation source and have only thermal sources. Boundary conditions are:

$$I^+(x, \mu, \tau = T) = 0 \quad ; \quad I^-(x, \mu, \tau = T) = 0$$

$$c = 10^{-3}, \quad B = 1 \quad (\text{throughout the medium})$$

The emergent intensity is plotted in figures 10 and 12 for optically thin and thick cases. The ratios of emergent source functions at different frequencies for the case $T = 155$ is given in table 2.

Table 2. Ratios of emergent source functions at different frequencies for $T = 155$

x	$S_L(R_V)/S_L(R_{II})$	$S_L(R_V)/S_L(R_{II})$
0.38	0.99	1.02
1.89	0.98	1.03
3.89	1.80	0.72
5.97	8.18	0.68

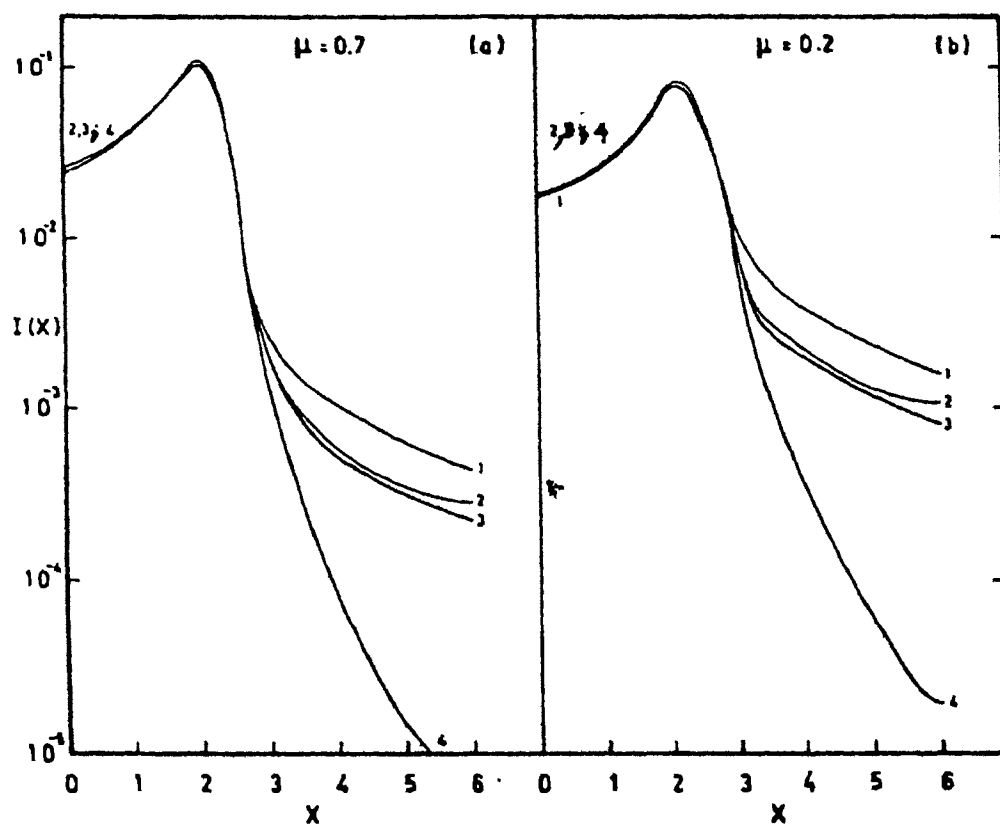


Figure 10' The emergent intensity for the case $\epsilon = 10^{-3}$, $\beta = 0$, $T = 155$ and no incident radiation on the boundaries. (a) $\mu = 0.7$ (b) $\mu = 0.2$. Numbers denote the following cases: (1) R_{III} , $a_j = 2 \times 10^{-3}$ (2) R_V , $a_1 = a_j = 10^{-3}$ (3) R_{III} , $a_j = 10^{-3}$ (4) R_{II} , $a_j = 2 \times 10^{-3}$

The partial coherency impedes the escape of photons through the wings. Therefore the efficiency of transfer of photons to the wings depends on the noncoherency of the redistribution mechanism. R_I and R_{III} being more noncoherent, transfer more photons to the wings. The result for R_{II} is in qualitative agreement with that of Hummer (1969) and R_{III} with that of Vardavas (1976b). Similar emergent profiles have been obtained by Hubeny and Heinzel (1984) but for $T = 10^4$ and $\epsilon = 10^{-4}$.

2.4.6. Continuous absorption

To see the effect of continuous absorption on line transfer with R_V redistribution, we consider certain cases with $\epsilon = \beta = 10^{-3}$ and $S_c = B = 1$. We also have some cases of very high optical depths of the order of 10^6 . We have covered a wide range of thermal sources. This kind of study is useful in understanding the formation of strong resonance lines like Ca II H and K, Hydrogen Lyman α etc. There is no input radiation to the medium. The frequency dependent source function at various optical depths is given in fig 13(a). Making use of the assumption $S_c = B$ and substituting equation (2.51) into equation (2.50) we have

$$S(x) = \frac{1 - \zeta(x)}{2 \phi(x)} \int_{-\infty}^{\infty} \int_{-1}^1 R(x', x) I(x', z, \mu') d\mu' dx' + \zeta(x)B \quad (2.52)$$

$$\text{where} \quad \zeta(x) = \frac{\beta + \epsilon \phi(x)}{\beta + \phi(x)} \quad (2.53)$$

In the far wings, $\zeta(x) \approx 1$ and therefore $S(x) \rightarrow B$ at all

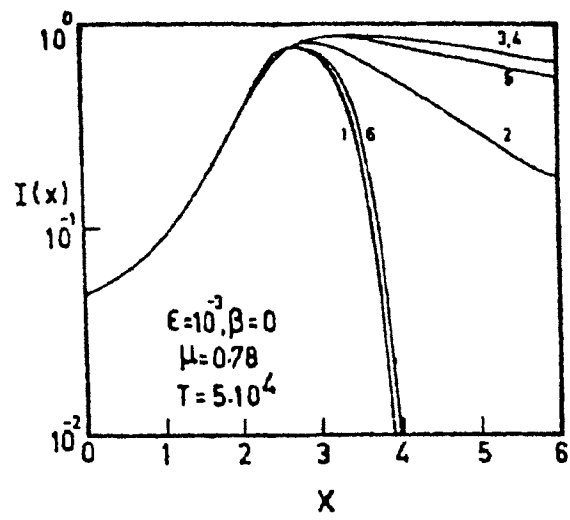


Figure 12 Same as figure 10 for $T = 5 \times 10^4$.
 numbers denote the following cases:
 (1) R_I (2) R_{II} (3) R_{III} (4) CRD with
 VAP (5) R_V (6) CRD with LAP.

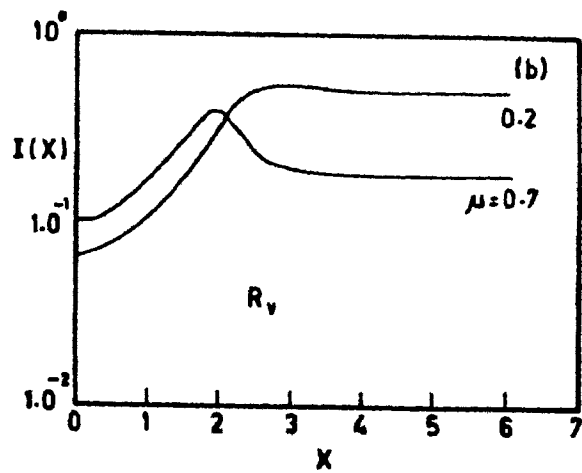
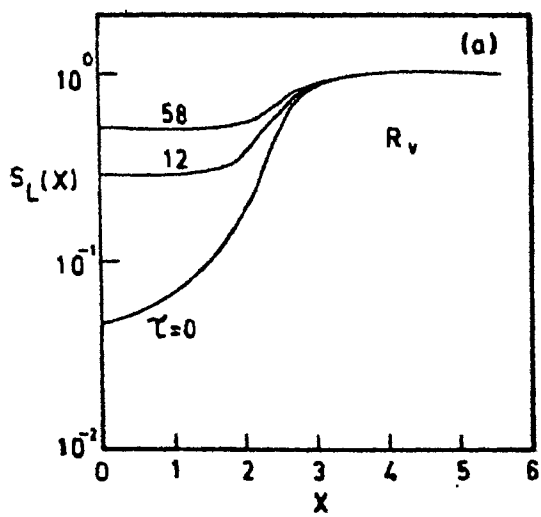
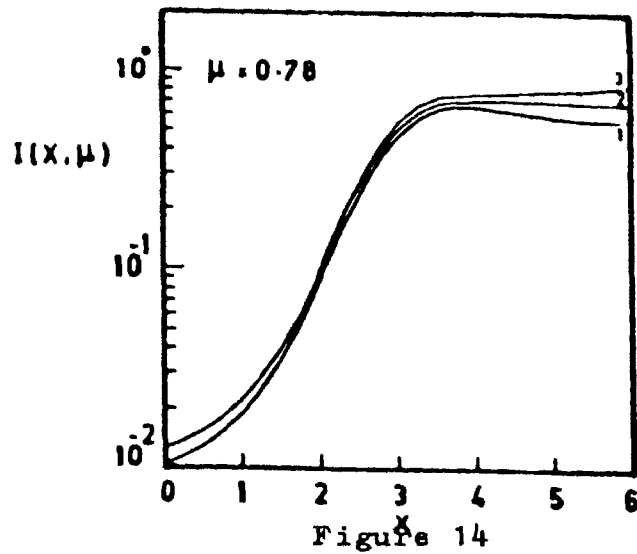
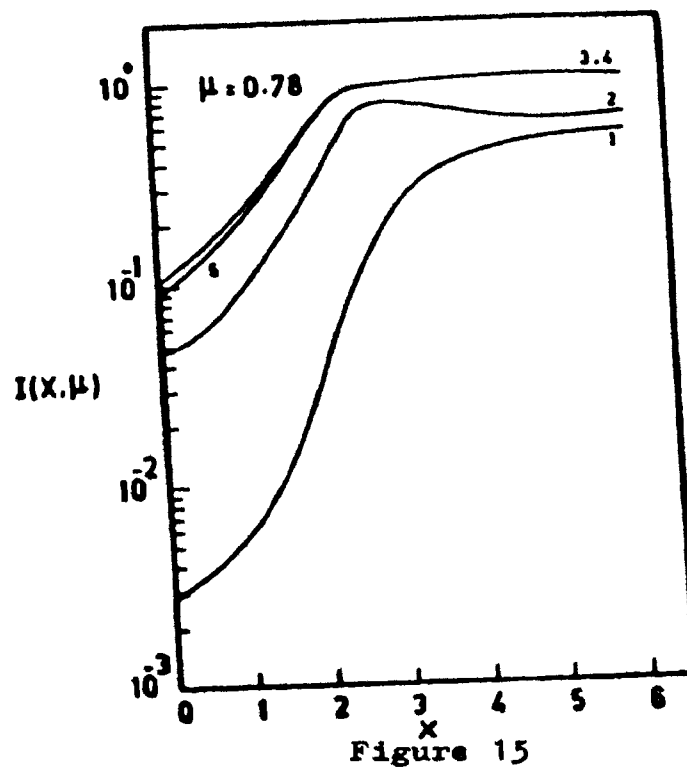


figure 13 (a) Source function for $\tau = 0, 12, \text{ and } 58$
 (b) Emergent intensities for R_V with $\epsilon = \beta = 10^{-3}$.



Emergent intensity plotted against frequency. (1) Medium with only thermal sources, R_{II} redistribution, total optical depth $T = 5 \cdot 10^4$, $\beta = 10^{-5}$, $\epsilon = 10^{-5}$ (2) same as (1) for R_{III} . (3) same as (1) for a medium with incident intensity as 1.



Same as figure 1 for (1) medium with incident intensity as 1, R_{II} , $T = 5 \cdot 10^4$, $\epsilon = \beta = 10^{-6}$. (2) same as (1) for $\beta = 0$, $\epsilon = 10^{-3}$ (3) same as (2) for $\beta = 10^{-3}$ (4) medium with only thermal sources, CRD with voigt absorption profiles, $T = 5 \cdot 10^4$, $\beta = \epsilon = 10^{-3}$ (5) same as (4) for R_{II} , $\beta = 10^{-3}$, $\epsilon = 10^{-5}$

optical depths. In the wings, the intensity can be approximated by $I(x, \mu) \approx B(\beta T) / \mu$. These characteristics are reflected both in source function (fig 13 (a)) as well as in the emergent intensity profiles (fig 13 (b)). We see from these figures that in the wings the line transfer is dominated by the overlying continuous absorption.

Keeping all the parameters like boundary condition, contribution from external source and continuous opacity same, we find R_{II} redistribution gives lesser intensity in the wing compared to R_{III} . Coherent nature of R_{II} redistribution function prohibits the photons which are absorbed at the line centre to be emitted in the wing. Therefore R_{II} redistribution function produces less intensity in the wing compared to R_{III} . If there is some input radiation at one boundary we find that the input escapes through the wings because the wings are optically thin. This drains the photons at the line centre and hence the intensity at the line centre is less compared to the case of pure thermal sources. The above characteristics are seen in figure 14.

The effects of continuous opacity and thermal sources are seen in figure 15. Continuous opacity generally makes the emergent intensity profile to be a weak line. When the continuous opacity is absent, a very weak emission reversal is also seen. We also get extended wings when the continuous opacity is absent. The line becomes weak because of the addition of continuous sources of photons which are emitted according to Planck distribution. When large amount of

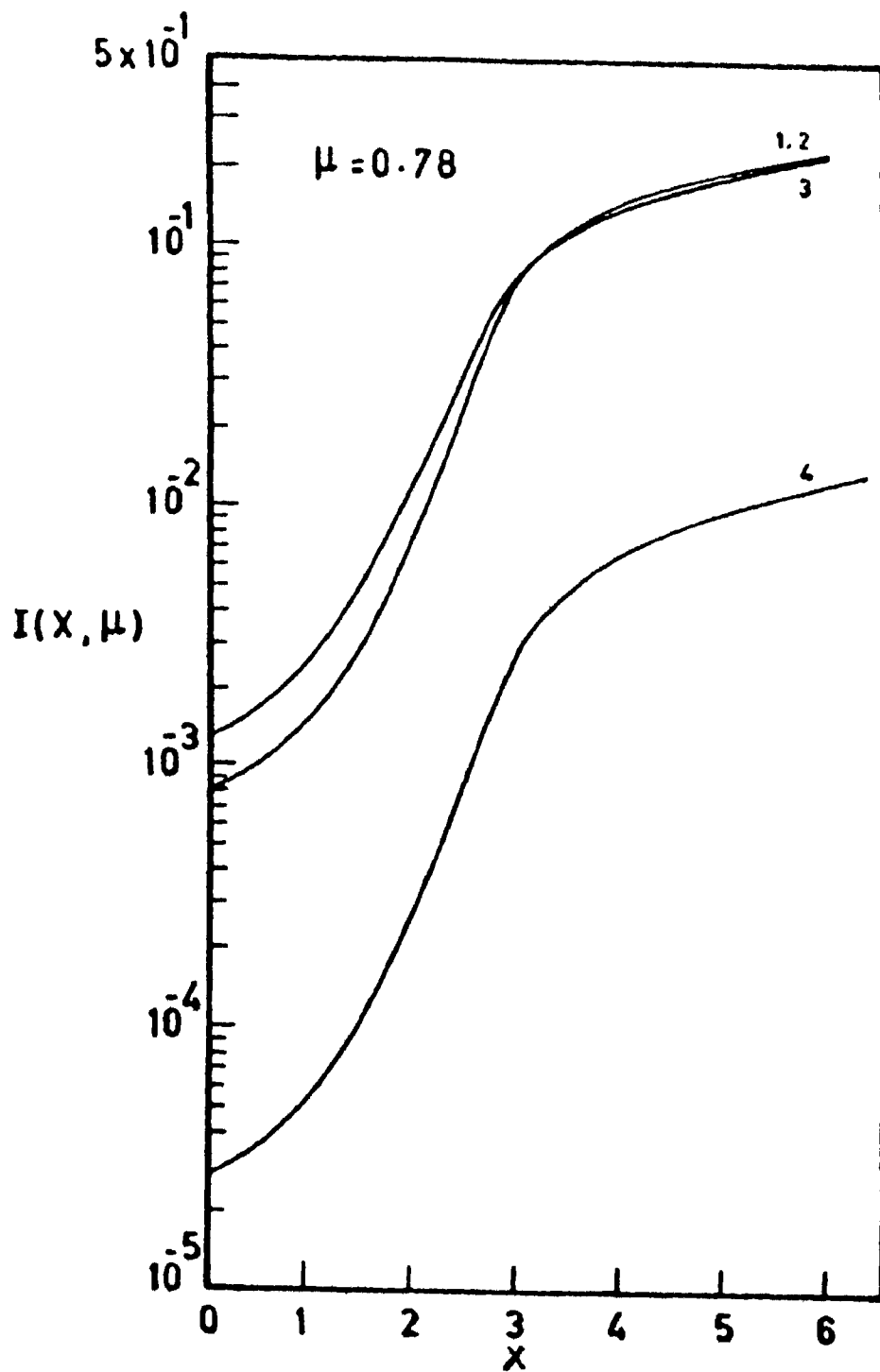


FIG.16

Same as figure (1) for (1) medium with incident intensity as 1, R_{II} , $T = 5 \cdot 10^6$, $\beta = 0$, $\epsilon = 10^{-6}$, (2) medium with only thermal sources, R_{II} , $T = 5 \cdot 10^6$, $\beta = 0$, $\epsilon = 10^{-6}$. (3) same as (2) for $\beta = 0$, $\epsilon = 10^{-6}$, (4) pure scattering medium with incident intensity as 1, R_{II} , $T = 5 \cdot 10^6$, $\beta = \epsilon = 0$.

continuous opacity and thermal sources are present, the line gets saturated and the higher optical depths do not affect the emergent intensity profile. When thermal sources are reduced, we find that the line centre intensity drops down. But the wing is unaltered. When the continuous opacity source is reduced, we get a deep absorption profile with broad wings. This effect is continued to be reflected in figure 16 also. R_{III} redistribution increases the line centre intensity because of the easy diffusion of photons from line wing to centre. We finally get a very deep absorption profile with very extended wing for purely scattering atmospheres with large optical depths.

CHAPTER 3

THE EFFECT OF COHERENT AND NON-COHERENT ELECTRON SCATTERING WITH ATOMIC PARTIAL FREQUENCY REDISTRIBUTION ON LINE FORMATION

3.1. Introduction

Compton (1923) put forward a suggestion that the scattering of light by electrons may account for the observed displacement of the lines in the solar spectrum towards the red near the limb. This is because the photons near the limb suffer more scattering than those near the centre. This idea was investigated by Dirac (1925) who derived the angle dependent redistribution function for the electron scattering taking into account the thermal motion of the electrons. He arrived at the conclusion that a shift of the lines can not be produced by such a scattering mechanism. Nevertheless it is a well known fact that the scattering of radiation by electrons plays an important role in the atmospheres of early stars due to the high number density of electrons. Electron scattering is one of the main source of opacity in these stars. Chandrasekhar (1948) drew attention to the possibility of broadening of lines by electron scattering. This was investigated by Münch (1948) who considered the case of a semi-infinite atmosphere in which an absorption line is formed, covered by a finite layer of electrons. With these assumptions, he obtained line profiles with shallower cores and

broader wings since the photons are scattered from the continuum into the line core. His assumption of the existence of an absorption line deep in the atmosphere and ignoring the effect of electrons was questioned by Gebbie and Thomas (1968). A more realistic situation is one in which scattering and absorption in the line, scattering by electrons and absorption in the continuum all occur simultaneously. Auer and Mihalas (1968) considered such a case. They assumed the electron scattering to be coherent and non-coherent and atomic scattering to be always described by a complete redistribution (CRD) mechanism for a Doppler absorption profile. If the electron scattering coefficient exceeds continuous absorption, they obtained measurable changes in the line profile between coherent and non-coherent electron scattering. For strong resonance lines formed in early type stars, one has to consider the partial frequency redistribution of photons by atoms as well as coherent or non-coherent scattering by electrons which they have not considered.

We have incorporated partial frequency redistribution (PRD) function of atoms into the calculations of spectral lines from the media in which atoms and electrons together participate in absorbing, emitting or scattering the photons. In this chapter, coherent and non-coherent electron scattering combined with complete and partial frequency redistribution by atoms is studied for parametrized models, so that the

underlying physics can be discerned. In the next section, we briefly describe the electron scattering function and in section 3.3 we give the detailed account of the method to solve the problem. In section 3.4 we discuss the results.

3.2. Electron scattering redistribution functions

The angle dependent laboratory frame redistribution function is given by (Mihalas, 1978),

$$R^e(\nu', \mathbf{n}', \nu, \mathbf{n}) = g(\mathbf{n}', \mathbf{n}) \left[\frac{mc^2}{4\pi kT(1-\cos\Theta)\nu^2} \right]^{\frac{1}{2}} \exp \left[\frac{-mc^2(\nu-\nu')^2}{4kT(1-\cos\Theta)\nu^2} \right] \quad (3.1)$$

This expression is valid for all wavelength regions of electromagnetic spectrum except for short wavelengths. In other words, the above formula can be applied in the limit that Compton effects are negligible (i.e. $\frac{h\nu}{mc^2} \ll 1$). ν', ν

are frequencies of the incoming and scattered waves. \mathbf{n}' and \mathbf{n} denote the incoming and scattered directions. k is the Boltzmann constant. c is velocity of light. m and T are the electron mass and temperature. Θ is the scattering angle. $g(\mathbf{n}', \mathbf{n})$ is the phase function which is normally assumed to be either isotropic or dipole.

The angle averaged redistribution function can be obtained by either integrating the expression given by

equation (3.1) or from the first principles. Auer and Mihalas (1968) derived the angle averaged redistribution function from the first principles. Here we give the alternate method:

To normalize the above equation we have to divide it by $16\pi^2$. (See equation 2.7 of Mihalas (1978)). Also substituting the following relations (assuming isotropic scattering)

$$w = \frac{v_0}{c} \sqrt{\frac{2kT}{m}} \quad ; \quad g(n', n) = 1$$

$$(1 - \cos \Theta) = 2 \sin^2 \Theta/2 \quad ; \quad (\nu - \nu') = \Delta\nu$$

we have for a normalized redistribution function

$$R(\nu', n'; \nu, n) = \frac{1}{32\pi^2 w\sqrt{\pi}} \frac{1}{\sin \Theta/2} \exp\left[-\frac{(\Delta\nu)^2}{4w^2 \sin^2 \Theta/2}\right] \quad (3.2)$$

$$R(\nu', \nu) = 8\pi^2 \int_0^\pi R(\nu', n'; \nu, n) \sin \Theta d\Theta \quad (3.3)$$

Angle averaging equation (3.2) using equation (3.3) we get

$$R(\nu', \nu) = \frac{1}{2w\sqrt{\pi}} \int_0^\pi e^{-\frac{(\Delta\nu)^2}{4w^2 \sin^2 \Theta/2}} \cos \Theta/2 d\Theta$$

Let $y = \sin \Theta/2$. Therefore,

$$R(\nu', \nu) = \frac{1}{w\sqrt{\pi}} \int_0^1 e^{-\frac{(\Delta\nu)^2}{4w^2 y^2}} dy$$

Let $(\Delta\nu)^2 / (4w^2y^2) = z^2$. Then R becomes

$$\begin{aligned}
 R(\nu', \nu) &= \frac{1}{w\sqrt{\pi}} \int_{|\Delta\nu|/2w}^{\infty} \frac{e^{-z^2}}{z^2} \frac{|\Delta\nu|}{2w} dz \\
 &= \frac{1}{w} \operatorname{ierfc} \left(\left| \frac{\nu' - \nu}{2w} \right| \right) \quad (3.4)
 \end{aligned}$$

where $\operatorname{ierfc}(z)$ is the integral of the complimentary error function.

$$\operatorname{ierfc}(z) = \int_z^{\infty} \operatorname{erfc}(x) dx = \frac{1}{\sqrt{\pi}} e^{-z^2} - z \operatorname{erfc}(z) \quad (3.5)$$

Finally the electron redistribution function as a function of frequencies expressed in atomic Doppler units is

$$R^e(x', x) = \left[\frac{1}{\omega} \right] \operatorname{ierfc} \left(\left| \frac{x - x'}{2\omega} \right| \right) \quad (3.6)$$

ω is the ratio of electron to atomic Doppler widths and is given by $\omega \approx 43 A^{1/2}$ where A is the atomic weight of the atom under consideration. ω is chosen as 80 which corresponds roughly to that of Helium atoms. x' and x are the frequencies of the absorbed and emitted photons expressed in atomic Doppler units. In Fig. 1 the function $R^e(\beta)$ is plotted against β where $\beta = |y - y'|$ and y and y' are frequencies expressed in electron Doppler units. We can not compare this with a function like Gaussian because that is a function of

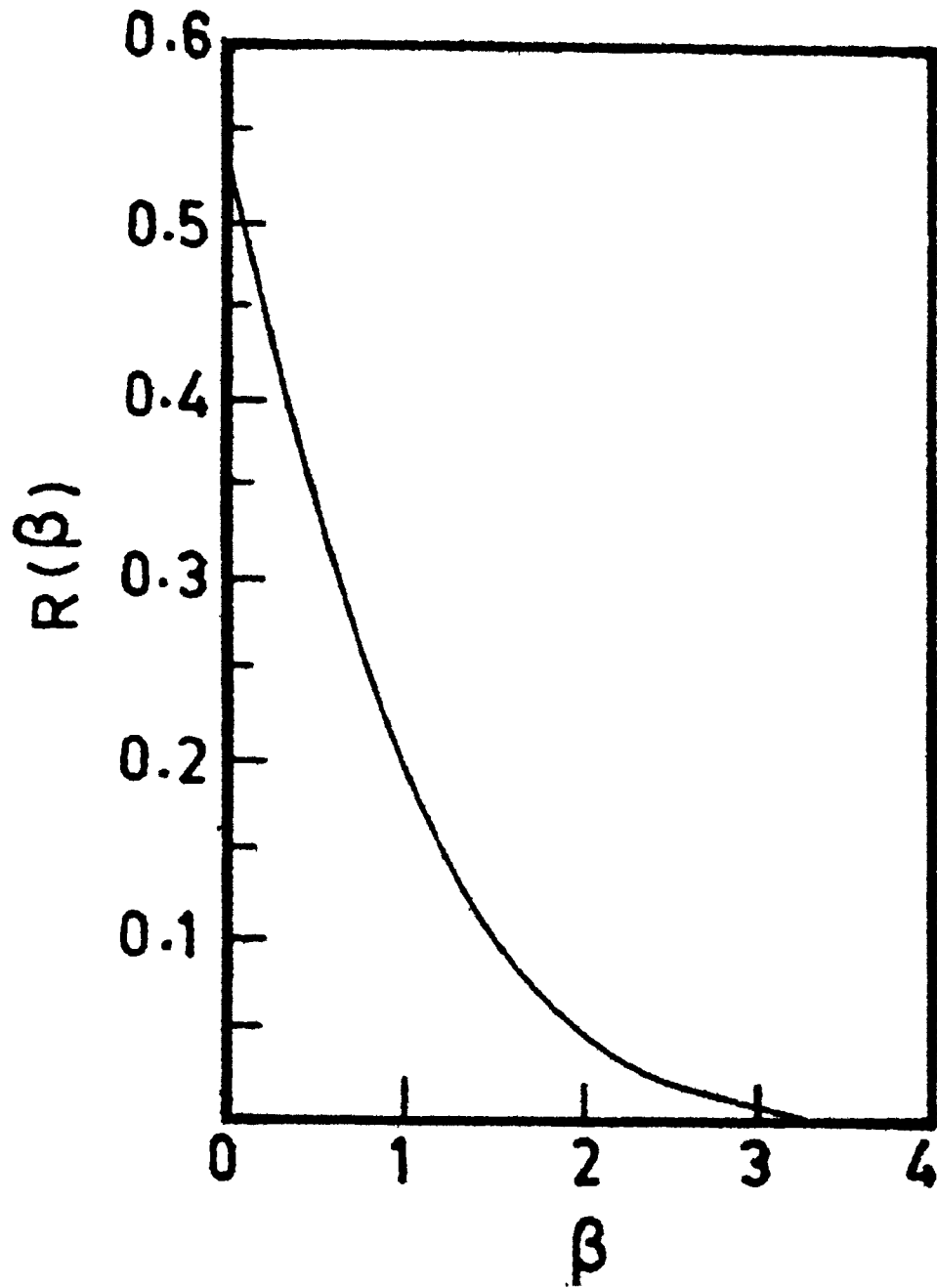


Figure 1 The angle averaged Redistribution function with isotropic phase function for electron scattering as a function of $\beta = |\nu - \nu'|/\omega$ where ω is the electron Doppler width to atomic Doppler width ratio.

frequency expressed in atomic Doppler units which is 80 times smaller than electron Doppler units and so falls off too steeply for comparison purposes. From now onwards superscript 'e' is used to denote electron redistribution and 'a' for atomic redistribution function.

Fig. 1 is in good agreement with that of Hummer and Mihalas (1967). Frequency expressed in atomic Doppler units enter in the calculations of radiative transfer. So, if we transform $R^e(y - y')$ to $R^e(x', x)$ we find that, over a few atomic Doppler widths, $R^e(x', x)$ remains constant. Therefore the contribution from non-coherent electron scattering remains constant in the Doppler core of the line. We also see from the Fig. 1 that the non-coherent electron scattering may influence in the wing to very large atomic Doppler units away from the line centre. This is due to the large ratio of electron to atomic Doppler widths.

3.3. Method of solution

The radiative transfer equation for a two level atom including noncoherent electron scattering is given by

$$\begin{aligned}
 \pm \mu \frac{dI(x, \pm \mu, z)}{dz} &= -(k_c + \sigma_e + \chi_{l_0} \phi(x)) I(x, \pm \mu, z) + \chi_{l_0} \phi(x) B \\
 &+ k_c B + \frac{1-\epsilon}{2} \chi_{l_0} \int_{-1}^{+1} \int_{-\infty}^{\infty} R^a(x', x) I(x', \mu', z) d\mu' dx' \\
 &+ \sigma_e \int_{-1}^{+1} \int_{-\infty}^{\infty} R^e(x', x) I(x', \mu', z) d\mu' dx' \quad (3.7)
 \end{aligned}$$

where k_c and σ_e are the continuous absorption and electron scattering coefficients for unit volume. χ_{l_0} is the atomic absorption coefficient at the line centre. ϵ, ϕ and B have the same meaning as in the previous chapter. $R^a(x', x)$ and $R^e(x', x)$ denote the atomic and electron redistribution functions respectively. For the problem of coherent electron scattering we have

$$R^e(x', x) dx' = \delta(x' - x) dx' \quad (3.8)$$

where $\delta(x' - x)$ denotes the Dirac delta function.

Though the above equation (3.7) is solved within the framework of Discrete space theory, the choice of quadrature points, normalization, segmenting the problem into core and wing regions and the iteration procedure are all followed according to Auer and Mihalas (1968). Since modification of the method due to Grant and Peraiah (1972) is necessary to tackle this problem, an account of the method is given below:

Defining

$$\beta_e = \frac{\sigma_e}{\chi_{l_0}}, \quad \beta_c = \frac{k_c}{\chi_{l_0}}, \quad \text{and} \quad \beta = \beta_e + \beta_c \quad \text{we get}$$

$$\begin{aligned} \pm \frac{\mu}{\chi_{l_0}} \frac{dI(x, \pm \mu, z)}{dz} &= - [\beta + \phi(x)] I(x, \pm \mu, z) + \epsilon \phi(x) B \\ &+ \frac{1-\epsilon}{2} \int_{-1}^1 \int_{-\infty}^{\infty} R^a(x', x) I(x', \mu', z) dx' d\mu' + \beta_c B \\ &+ \frac{\beta_e}{2} \int_{-1}^1 \int_{-\infty}^{\infty} R^e(x', x) I(x', \mu', z) dx' d\mu' \end{aligned} \quad (3.9)$$

Since this problem has symmetric solution with respect to the line centre, we need to consider only half the frequency grid.

$$\begin{aligned}
 \pm \frac{\mu}{x_{l_0}} \frac{dI(x, \pm \mu, z)}{dz} &= - [\beta + \phi(x)] I(x, \pm \mu, z) + \phi(x) B \\
 + \frac{1-\epsilon}{2} \int_{-1}^1 \int_0^{\infty} [R^a(x', x) + R^a(-x', x)] I(x', \mu', z) dx' d\mu' &+ \beta_c B \\
 + \frac{\beta_e}{2} \int_{-1}^1 \int_0^{\infty} [R^e(x', x) + R^e(-x', x)] I(x', \mu', z) dx' d\mu' &
 \end{aligned}
 \tag{3.10}$$

The frequency integration is split into two regions. One is the core region where the interval is $[0, x_0]$ and the other is the wing region where the interval is $[x_0, \infty]$. Reason for such a demarkation is due to the fact that the problem is characterized by two intrinsic frequency scales, one for the atoms and the other for electrons. Coverage in the line must be fine enough for taking the atomic redistribution into account. Coverage in the wings should extend to 4 electron Doppler widths which correspond to around 320 atomic Doppler widths. Here the frequency quadrature can have a larger mesh size. Hence the equation is split into two parts, one for the core and the other for the wing region. The equation for the core region can be written as

$$\begin{aligned}
\pm \frac{\mu}{x_0} \frac{dI(x, \pm \mu, z)}{dz} &= - [\beta + \phi(x)] I(x, \pm \mu, z) + \epsilon \phi(x) B \\
+ \frac{1-\epsilon}{2} \int_{-1}^1 \int_0^{x_0} &\left[R^a(x', x) + R^a(-x', x) \right] I(x', \mu', z) dx' d\mu' + \beta_c B \\
+ \frac{\beta_e}{2} \int_{-1}^1 \int_0^{x_0} &\left[R^e(x', x) + R^e(-x', x) \right] I(x', \mu', z) dx' d\mu' + D^1(x, z)
\end{aligned}$$

0 ≤ x ≤ x₀ = 5 (3.11)

where

$$\begin{aligned}
D^1(x, z) &= \frac{1-\epsilon}{2} \int_{-1}^1 \int_{x_0}^{\infty} \left[R^a(x', x) + R^a(-x', x) \right] I(x', \mu', z) dx' d\mu' \\
&+ \frac{\beta_e}{2} \int_{-1}^1 \int_{x_0}^{\infty} \left[R^e(x', x) + R^e(-x', x) \right] I(x', \mu', z) dx' d\mu'
\end{aligned}$$

(3.12)

In the above equation, the first term on the right hand side denotes the continuous absorption. The second term represents the thermal sources and the first scattering integral denotes the photons which are reshuffled within the spectral line by the atomic scattering process. Next term is the contribution from the continuous sources to the pool of photons. The second scattering integral represents the photons which are reshuffled by electron scattering process. The term D^1 is described after equation (3.14) in the text. For the wing region the transfer equation becomes

$$\begin{aligned}
\pm \frac{\mu}{x_0} \frac{dI(x, \pm \mu, z)}{dz} &= - [\beta + \phi(x)] I(x, \pm \mu, z) + \epsilon \phi(x) B \\
+ \frac{1-\epsilon}{2} \int_{-1}^1 \int_{x_0}^{\infty} &\left[R^a(x', x) + R^a(-x', x) \right] I(x', \mu', z) dx' d\mu' + \beta_c B \\
+ \frac{\beta_e}{2} \int_{-1}^1 \int_{x_0}^{\infty} &\left[R^e(x', x) + R^e(-x', x) \right] I(x', \mu', z) dx' d\mu' + D^2(x, z)
\end{aligned}$$

$x_0 \leq x \leq \infty \quad (3.13)$

where

$$\begin{aligned}
D^2(x, z) &= \frac{1-\epsilon}{2} \int_{-1}^1 \int_0^{x_0} \left[R^a(x', x) + R^a(-x', x) \right] I(x', \mu', z) dx' d\mu' \\
&+ \frac{\beta_e}{2} \int_{-1}^1 \int_0^{x_0} \left[R^e(x', x) + R^e(-x', x) \right] I(x', \mu', z) dx' d\mu'
\end{aligned}$$

(3.14)

In the above equations x_0 marks the division between the core and the wing. D^1 and D^2 are respectively the source terms for photons being scattered from the wings into the core and from the core into the wings. Equations (3.11) and (3.13) are coupled together through D^1 and D^2 terms. This coupling arises due to the noncoherent electron scattering which redistributes the photons from the core to the wing and wing to the core of the spectral line. Following Auer and Mihalas (1968) the interval $[x_0, \infty]$ is limited to $[x_0, x_1]$ and the remainder is handled analytically assuming $I_x = I_{x_1}$ for $x > x_1$ so that I_x may be taken out of the integral. Mathematically this reduces to

$$\begin{aligned}
& \int_{-1}^1 \int_{x_0}^{\infty} \left[R^E(x', x) + R^E(-x', x) \right] I(x', \mu', z) dx' d\mu' \\
&= \int_{-1}^1 \int_{x_0}^{x_1} \left[R^E(x', x) + R^E(-x', x) \right] I(x', \mu', z) dx' d\mu' \\
&+ \int_{-1}^1 I(x', \mu', z) d\mu' \int_{x_1}^{\infty} \left[R^E(x', x) + R^E(-x', x) \right] dx' \\
&= \int_{-1}^1 \int_{x_0}^{x_1} \left[R^E(x', x) + R^E(-x', x) \right] I(x', \mu', z) dx' d\mu' \\
&+ 2 \left[i^2 \operatorname{erfc} \left| \frac{x - x_1}{2w} \right| + i^2 \operatorname{erfc} \left| \frac{x + x_1}{2w} \right| \right] \int_{-1}^1 I(x', \mu', z) d\mu'
\end{aligned} \tag{3.15}$$

where

$$i^2 \operatorname{erfc}(z) = \int_z^{\infty} i \operatorname{erfc}(z') dz' = \frac{1}{2} \left[z^2 + \frac{1}{2} \right] \operatorname{erfc}(z) - \frac{ze^{-z^2}}{2\sqrt{\pi}} \tag{3.16}$$

The integrals are reduced to summation over weighted values of the function. The equation (3.9) can be written at frequency x_i and μ_j and depth z_n as

$$\begin{aligned}
\pm \frac{\mu_j}{\chi_{20}} \frac{dI_{i,j,n}^{\pm}}{dz} = & - \left[\beta_n + \phi_{i,n} \right] I_{i,j,n}^{\pm} + \epsilon_n \phi_{i,n} E_n + \beta_{i,n} E_n \\
& + \frac{(1 - \epsilon_n)}{2} \sum_{i'=1}^I \sum_{j'=1}^J R_{i',i}^a a_{i',j'} C_{j'} \left[I_{i',j',n}^+ + I_{i',j',n}^- \right] \\
& - \frac{\beta_{E,n}}{2} \sum_{i'=1}^I \sum_{j'=1}^J R_{i',i}^a a_{i',j'} C_{j'} \left[I_{i',j',n}^+ + I_{i',j',n}^- \right] + D_{i,n}^{1,2}
\end{aligned} \tag{3.17}$$

I^+ and I^- are two oppositely directed beams. Defining

$$\begin{aligned}
I_{i,j,n}^{\pm} &= I^{\pm}(x_i, \pm \mu_j, z_n) \\
R_{i',i}^{a,E} &= R^{a,E}(x_{i'}, x_i) + R^{a,E}(-x_{i'}, x_i) \\
\phi_{i,n} &= \phi(x_i, z_n)
\end{aligned} \tag{3.18}$$

$$I_{i,n}^{\pm} = \begin{bmatrix} I^{\pm}(x_i, \pm \mu_1, z_n) \\ I^{\pm}(x_i, \pm \mu_2, z_n) \\ \vdots \\ I^{\pm}(x_i, \pm \mu_J, z_n) \end{bmatrix}_{J \times 1}$$

$$C_m = \begin{bmatrix} c_1 & c_2 & \dots & c_J \\ c_1 & c_2 & \dots & c_J \\ \dots & \dots & \dots & \dots \\ c_1 & c_2 & \dots & c_J \end{bmatrix}_{J \times J} \quad ; \quad M_m = \mu_j \delta_{jk}$$

where J and I are the total number of angles and frequencies considered in the region of the spectral line.

$$\begin{aligned} \frac{M_m}{\chi_{lo}} \frac{dI_{i,n}^{\pm}}{dz} = & - \left[\beta + \phi_{i,n} \right] I_{i,n}^{\pm} + \epsilon \phi_{i,n} B_n + \beta_c B_n \\ & + \frac{(1-\epsilon)}{2} \sum_{i'=1}^I R_{i',i}^a \alpha_{i'} C_m \left[I_{i',n}^{\pm} + I_{i',n}^{\pm} \right] \\ & + \frac{\beta_n}{2} \sum_{i'=1}^I R_{i',i}^e \alpha_{i'} C_m \left[I_{i',n}^{\pm} + I_{i',n}^{\pm} \right] + D_{i,n}^{1,2} \end{aligned} \quad (3.19)$$

Integrating the above equations over the depth interval $[z_n, z_{n+1}]$ we have

$$\begin{aligned} M_m (I_{i,n+1}^+ - I_{i,n}^+) + \tau_{n+1/2} (\beta + \phi_i) I_{i,n+1/2}^+ \\ = \tau_{n+1/2} (\beta_c + \epsilon \phi_i) B_{n+1/2} + \tau_{n+1/2} D_{i,n+1/2}^{1,2} \\ + \beta_{e,n+1/2} \tau_{n+1/2} \sum_{i'=1}^I R_{i',i}^e \alpha_{i'} C_m (I_{i,n+1/2}^+ + I_{i,n+1/2}^-) \\ + \frac{(1-\epsilon)}{2} \tau_{n+1/2} \sum_{i'=1}^I R_{i',i}^a \alpha_{i'} C_m (I_{i,n+1/2}^+ + I_{i,n+1/2}^-) \end{aligned} \quad (3.20)$$

and

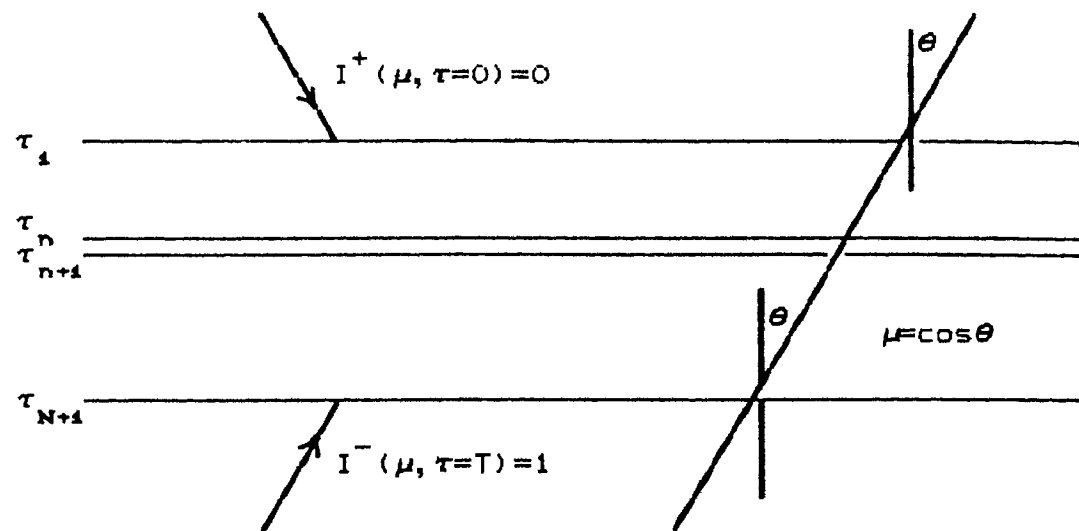
$$\begin{aligned} M_m (I_{i,n}^- - I_{i,n+1}^-) + \tau_{n+1/2} (\beta + \phi_i) I_{i,n+1/2}^- \\ = \tau_{n+1/2} (\beta_c + \epsilon \phi_i) B_{n+1/2} + \tau_{n+1/2} D_{i,n+1/2}^{1,2} \\ + \beta_{e,n+1/2} \tau_{n+1/2} \sum_{i'=1}^I R_{i',i}^e \alpha_{i'} C_m (I_{i,n+1/2}^+ + I_{i,n+1/2}^-) \\ + \frac{(1-\epsilon)}{2} \tau_{n+1/2} \sum_{i'=1}^I R_{i',i}^a \alpha_{i'} C_m (I_{i,n+1/2}^+ + I_{i,n+1/2}^-) \end{aligned} \quad (3.21)$$

Here the optical depth τ is defined as

$$\tau_{n+1/2} = \chi_{lo,n+1/2} \Delta z \quad (3.22)$$

$n, n+1$ and $n+1/2$ refer to quantities at τ_n , τ_{n+1} and $\tau_{n+1/2}$ where $n+1/2$ refers to the average over the shell in the medium

bounded by the layers τ_n and τ_{n+1} . Physical quantities like the absorption χ , intensity I etc are averaged. M_m contains angular quadrature roots and the matrices a and C contain frequency and angular quadrature weights. The geometry with the boundary conditions chosen is given in the following diagram.



In the above equations we can combine the angular and frequency quadrature weights as

$$w_k = a_i c_j \quad (3.23)$$

$$(i,j) \equiv k \equiv j + (i-1)j \quad 1 \leq k \leq K = i \times j$$

Here i and j refer to frequency and angular points. There are i total number of frequency and j total number of angular points chosen. Profile function and the redistribution functions were suitably normalized according to the procedure outlined by Auer and Mihalas (1968).

Let us define the following quantities:

$$I_n^\pm = \left[I_k^\pm \right]_n, \quad \phi_{n+1/2} = \left[\beta + \phi_k \right]_{n+1/2} \delta_{kk'} \quad (3.24)$$

$$S_{n+1/2} = (\beta + \epsilon \phi_k)_{n+1/2} B_{n+1/2} \delta_{kk'} + D_{n+1/2}^{1,2}$$

3.3.1. Definition of R^e and D matrices for coherent and non-coherent electron scattering

Coherent electron scattering :

Since the terms in D are small we first set the D vector to be a zero vector. R^e is given by

$$R^e = \frac{\beta_e}{2} \begin{bmatrix} R_j & & 0 \\ & R_j & \\ 0 & & R_j \end{bmatrix}_{ixi} \quad (3.25)$$

where i is the total number of frequency points in the region considered.

$$R_j = \begin{bmatrix} 1 & 1 & \dots & \dots & 1 \\ 1 & 1 & \dots & \dots & 1 \\ \dots & \dots & \dots & \dots & \dots \\ 1 & 1 & \dots & \dots & 1 \end{bmatrix}_{jxj} \quad (3.26)$$

where j is the total number of angles considered. Here core and wing are decoupled from each other as far as the electron redistribution is concerned. So the equations (3.11) and (3.13) can be solved separately without involving any iteration scheme.

Non-coherent electron scattering :

First iteration ; Core solution

Let us denote the number of frequencies in the core and the wing as \mathbf{x} and \mathbf{x}_1 respectively. Then

$$D_{n+1/2}^1 = \frac{\beta_e}{2} [d_k^1]_{\mathbf{x}} ; d_k^1 = 0 \quad (3.27)$$

Here D^1 is a zero vector because of lack of information about the wing solution in the first instance. To evaluate the D^1 term, we should know the radiation field in the wing. Since we have not yet solved for the radiation field in the wing, we make this term a zero vector in the first iteration. To compensate for this, we add an extra term to the \mathbf{i}^{th} column in the R^e matrix which is described below:

$$R^e = \begin{bmatrix} R_j & R_j & \dots & R_j \\ \vdots & \vdots & & \vdots \\ R_j & R_j & \dots & R_j \end{bmatrix}_{\mathbf{ixi}} \quad (3.28)$$

Now the \mathbf{i}^{th} column block in the R^e matrix becomes

$$(R_j)_{i,\mathbf{i}} = (R_j)_{i,\mathbf{i}} + 2 \left[i^2 \operatorname{erfc} \left| \frac{x_i - x_1}{2w} \right| + i^2 \operatorname{erfc} \left| \frac{x_i + x_1}{2w} \right| \right]_{x_i \leq x_0} \quad (3.29)$$

where $(R_j)_{i,i}$ in the R.H.S. are the usual electron redistribution values. The extra term corresponds to a constant value assumed for the specific intensity in the wings which is equal to its value at the last point in the core. The above equations (3.27-3.29) are used in equation (3.11) to obtain the core solution.

First iteration ; wing solution

The term D^2 occurring in equation (3.13) becomes D_i^2 in equations (3.20) and (3.21) which is evaluated in the following way:

$$D^2 = \begin{bmatrix} d_1^2 \\ d_2^2 \\ \cdot \\ d_{I_1}^2 \end{bmatrix}_{I_1 \times I_1} \quad d_i^2 = \begin{bmatrix} d^2(x_i, \mu_1) \\ d^2(x_i, \mu_2) \\ \cdot \\ d^2(x_i, \mu_j) \end{bmatrix}_{j \times I_1} \quad (3.30)$$

$$d_i^2 = \sum_{i'=1}^I \sum_{j'=1}^J \left[R^e(x_i, x_{i'}) + R^e(x_i, -x_{i'}) \right] \alpha_{i',c_{j'}} (I_{i',j'}^{+e} + I_{i',j'}^{-e})$$

$$x_0 \leq x_i \leq x_{I_1} \quad (3.31)$$

where the superscript e on I^+ and I^- refers to the core solution obtained in the present iteration.

$$R^e(x_i, x_{I_1}) = R^e(x_i, x_{I_1}) + R^e(x_i, -x_{I_1}) + 2 \left[i^2 \operatorname{erfc} \left| \frac{x_i - x_{I_1}}{2w} \right| \right. \\ \left. + i^2 \operatorname{erfc} \left| \frac{x_i + x_{I_1}}{2w} \right| \right] \quad (3.32)$$

The last term in equation (3.32) corresponds to the analytical term from equation (3.15). Equations (3.30-3.32) are used in the R.H.S of equation (3.13) to solve for the radiation field in the wing region of the line. One can very easily recognise that equation (3.31) is nothing but the discretized form of equation (3.14). The terms corresponding to R^a have been dropped because those matrix elements are very small.

Second iteration ; Core solution

In this case

$$D^1 = \begin{bmatrix} d_1^1 \\ d_2^1 \\ \vdots \\ d_I^1 \end{bmatrix} \quad d_i^1 = \begin{bmatrix} d^1(x_i, \mu_1) \\ \vdots \\ d^1(x_i, \mu_J) \end{bmatrix} \quad (3.33)$$

$$d_i^1 = \sum_{i'=1}^{I-1} \sum_{j'=1}^J (R^E(x_i, x_{i'}) + R^E(x_i, x_{i'})) \alpha_{i'} c_{j'} (I_{i'j'}^{+w} + I_{i'j'}^{-w}) \quad (3.34)$$

$$0 \leq x_i \leq x_0$$

where $R^E(x_i, x_{i'})$ is given by equation (3.32). The superscript w on I^+ and I^- refers to the wing solutions of the previous iteration. α is the quadrature weights. Now $R^E(x_i, x_{i'})$ does not contain any extra term because equation (3.34) takes into account the wing contribution to the core solution in the scattering integral.

Second iteration ; wing solution

d_i^2 and R^e 's are defined as in equation (3.31) and (3.32)

Higher iterations

For the core solution, equation (3.34) and for wing solution, quantities given by equations (3.31) and (3.32) are followed. x_0 is chosen as 5 and x_1 as 320. Frequency quadrature roots and weights are chosen according to Auer and Mihalas (1968). The iterations of the solutions for the core and wing parts are carried out till a convergence is reached for the frequency x_0 between core and wing solutions. Typically 5 iterations are required; 3 for core and 2 for wing solutions.

Now putting the terms in the equations (3.20) and (3.21) into matrix form and using the matrix definitions of (3.24) we obtain

$$M \left[I_{n+1}^+ - I_n^+ \right] + \tau_{n+1/2} \phi_{n+1/2} I_{n+1/2}^+ = \tau_{n+1/2} S_{n+1/2} + \frac{(1-\epsilon)}{2} \tau_{n+1/2} \left[R^a W (I^+ + I^-)_{n+1/2} \right] + \frac{\beta_e}{2} \tau_{n+1/2} \left[R^e W (I^+ + I^-)_{n+1/2} \right] \quad (3.35)$$

$$M \left[I_n^- - I_{n+1}^- \right] + \tau_{n+1/2} \phi_{n+1/2} I_{n+1/2}^+ = \tau_{n+1/2} S_{n+1/2} + \frac{(1-\epsilon)}{2} \tau_{n+1/2} \left[R^a W (I^+ + I^-)_{n+1/2} \right] + \frac{\beta_e}{2} \tau_{n+1/2} \left[R^e W (I^+ + I^-)_{n+1/2} \right] \quad (3.36)$$

where

$$M = \begin{bmatrix} M_m & & & \\ & M_m & & \\ & & \ddots & \\ & & & M_m \end{bmatrix} \quad (3.37)$$

using the Diamond rule, viz,

$$I_{n+1/2}^{\pm} = \frac{1}{2} (I_n^{\pm} + I_{n+1/2}^{\pm}) \quad (3.38)$$

Equations (3.35) and (3.36) can be combined to give

$$\begin{aligned} & \begin{bmatrix} M+\frac{\tau}{2} \left[\phi - \frac{\delta}{2} R^{\alpha W} - \frac{\beta_{\bullet}^{\tau}}{2} R^{\bullet W} \right] & - \frac{\delta\tau}{4} R^{\alpha W} - \frac{\beta_{\bullet}^{\tau}}{4} R^{\bullet W} \\ - \frac{\delta\tau}{4} R^{\alpha W} - \frac{\beta_{\bullet}^{\tau}}{4} R^{\bullet W} & M+\frac{\tau}{2} \left[\phi - \frac{\delta}{2} R^{\alpha W} - \frac{\beta_{\bullet}^{\tau}}{2} R^{\bullet W} \right] \end{bmatrix} * \begin{bmatrix} I_{n+1}^{+} \\ I_n^{-} \end{bmatrix} \\ = & \begin{bmatrix} M-\frac{\tau}{2} \left[\phi - \frac{\delta}{2} R^{\alpha W} - \frac{\beta_{\bullet}^{\tau}}{2} R^{\bullet W} \right] & \frac{\delta\tau}{4} R^{\alpha W} + \frac{\beta_{\bullet}^{\tau}}{4} R^{\bullet W} \\ \frac{\delta\tau}{4} R^{\alpha W} + \frac{\beta_{\bullet}^{\tau}}{4} R^{\bullet W} & M-\frac{\tau}{2} \left[\phi - \frac{\delta}{2} R^{\alpha W} - \frac{\beta_{\bullet}^{\tau}}{2} R^{\bullet W} \right] \end{bmatrix} * \begin{bmatrix} I_n^{+} \\ I_{n+1}^{-} \end{bmatrix} \\ & + \begin{bmatrix} S \\ S \end{bmatrix} \end{aligned} \quad (3.39)$$

Defining the following auxiliary matrices

$$P = \frac{\tau}{2} \left[\frac{\delta}{2} R^a W + \frac{\beta}{2} R^e W \right] ; \quad G = \frac{\tau}{2} \phi - P ; \quad (3.40)$$

$$Q = M + G ; \quad T = M - G ; \quad \Delta = \left[P^{-1}Q - Q^{-1}P \right]^{-1}$$

equation (3.39) can be rewritten as

$$\begin{bmatrix} I_{n+1}^+ \\ \\ \\ I_n^- \end{bmatrix} = \begin{bmatrix} t(n+1,n) & r(n,n+1) \\ \\ \\ r(n+1,n) & t(n,n+1) \end{bmatrix} \begin{bmatrix} I_n^+ \\ \\ \\ I_{n+1}^- \end{bmatrix} + \begin{bmatrix} \Sigma^+ \\ \\ \\ \Sigma^- \end{bmatrix} \quad (3.41)$$

Transmission (t) and reflection (r) matrices now become

$$t(n+1,n) = t(n,n+1) = \Delta \left[P^{-1}T + Q^{-1}P \right]$$

$$r(n+1,n) = r(n,n+1) = \Delta \left[I + Q^{-1}T \right]$$

and the internal source vectors

$$\Sigma^- = \Sigma^+ = \Sigma = \tau \Delta \left[P^{-1} + Q^{-1} \right]$$

where I refers to the identity matrix of suitable size. Now the equations are in the standard form to use the Discrete space theory technique described by Grant and Hunt (1969 a,b).

A detailed account of this procedure is given by Peraiah (1971). The numerical method described so far is codified into a computer program to obtain the solution.

3.4. Results and discussion

The method outlined in section 3.3 is quite general and can handle any arbitrary variation of all the parameters. The specific intensity obtained has second order accuracy. Computer memory and time are probably the constraints in using this method. These problems are overcome with the advent of fast computers having virtual memory operating systems.

Boundary conditions chosen are:

$$I^-(\tau_{N+1}, \mu) = 1 \quad ; \quad I^+(0, \mu) = 0$$

for all frequencies.

Two different optical depths are chosen. One corresponds to effectively optically thin ($T = 155$) and the other optically thick ($T = 5 \times 10^4$) situations. Criterion for effectively optically thick and thin are given in chapter 2. The ratio of continuous absorption to line absorption (β_c) is chosen as 0 and 10^{-3} . Different ratios of electron scattering to line absorption coefficients are considered ($\beta_e = 10^{-2}, 10^{-3},$ and 10^{-4}). Both coherent and non-coherent electron scattering with CRD and PRD for redistribution by atoms are the different physical situations considered.

3.4.1. Coherent electron scattering without continuous absorption

The emergent mean intensity as a function of frequency for coherent electron scattering media where redistribution of photons by atoms is either partial or complete is given in Fig. 2. In the following discussion, the core means Doppler core measured in atomic Doppler widths and not the core solution referred to, in section 3.3. The result for CRD with Doppler absorption profile (DAP) is in complete agreement with that of Auer and Mihalas (1968). For high optical depth media, we see that the partial frequency redistribution R_{II} , R_{III} and R_V give higher mean intensity in the wings compared to CRD with Doppler absorption profile. Although the above functions have Voigt absorption profile (VAP) which increases the opacity in the wings substantially, the probability that a photon is scattered from the core into the wings is also strongly increased. Hence there is higher mean intensity in the wings for the redistribution functions. Among the profiles given by the PRD functions, we find that the more non-coherent the redistribution is, the higher the value of mean intensity in the wings. This is due to the fact that the non-coherency increases the transfer of photons from the core to the wing. For an optically thin medium, ($T = 155$) the wings are transparent, and the directly transmitted radiation dominates the solution. This being almost the same for all

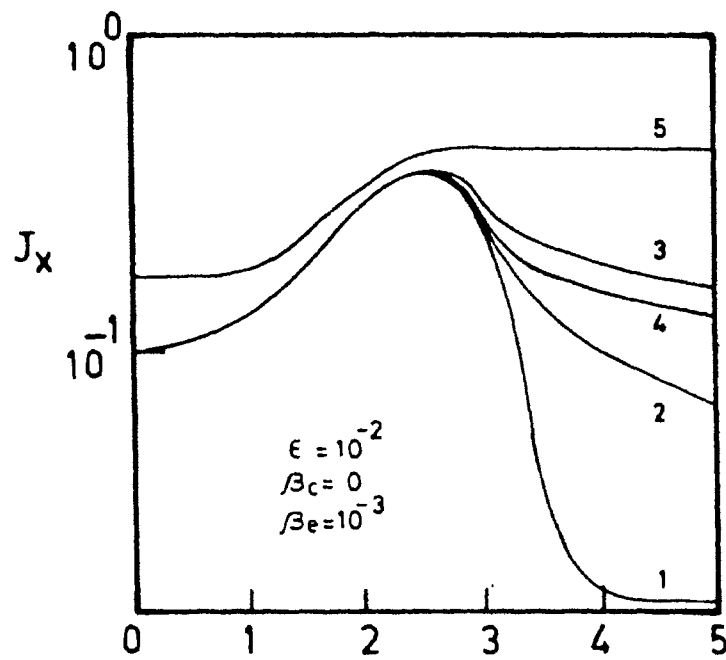


Figure 2 The emergent mean intensity for coherent electron scattering with $\epsilon = 10^{-2}$, $\beta_c = 0$, $\beta_e = 10^{-3}$. The abscissa gives frequencies measured in atomic Doppler widths. The numbers denote the following cases: (1) CRD with Doppler absorption profile (DAP) for $T = 5 \times 10^4$ (2) R_{II} (3) R_{III} (4) R_V (5) CRD with DAP, R_I , R_{II} , for $T = 155$.

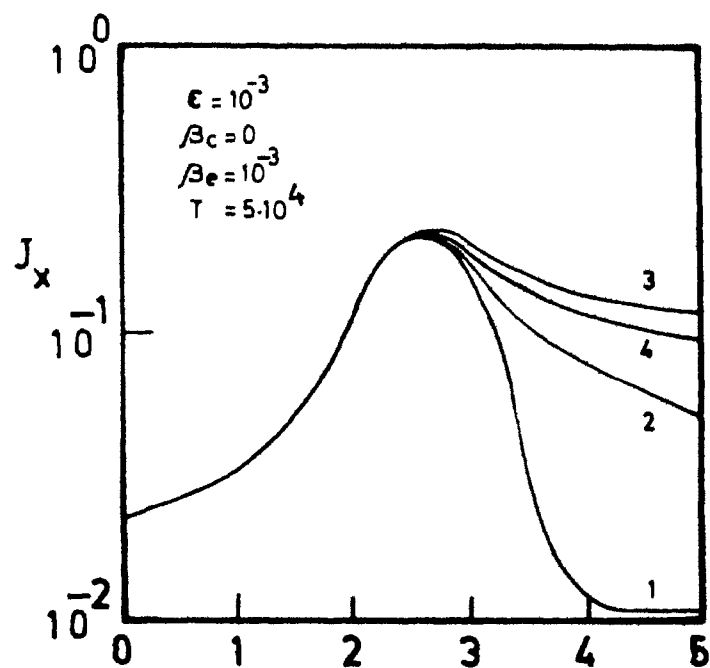


Figure 3 Same as fig.2 with $\epsilon = 10^{-3}$. The numbers denote the following cases: (1) R_I , CRD with DAP (2) R_{II} (3) CRD with Voigt absorption profile (VAP) (4) R_V .

redistribution functions, emergent profiles obtained are graphically unresolvable. When the thermal sources are decreased ($\epsilon = 10^{-2}$ to 10^{-3}) The same trend is retained with a decrease in mean intensity throughout the profile which can be seen from Figure 3.

3.4.2. The effect of continuous absorption with coherent electron scattering

In Figures 4-8, the ordinate gives emergent fluxes in units of continuum and the abscissa gives the frequency relative to the line centre in atomic Doppler widths. The result for DAP (Fig 4) is in quantitative agreement with that of Auer and Mihalas (1968). For optically thick media, the line develops an emission hump when the electron scattering is more than the continuous absorption irrespective of the redistribution mechanism employed (Fig. 4). In the wings the opacity is mainly due to continuous absorption and electron scattering. The line core appears in absorption due to scattering. The scattering pumps the photons from the core to other frequencies. The transition region between the core and the wing receives substantial amount of photons from the core. The contribution from the core falls off in the wing and also the continuous absorption and electron scattering decreases the intensity in the wing. Hence we see an emission hump in the transition region. When the total optical depth of the medium is reduced, we see almost an absorption line with a

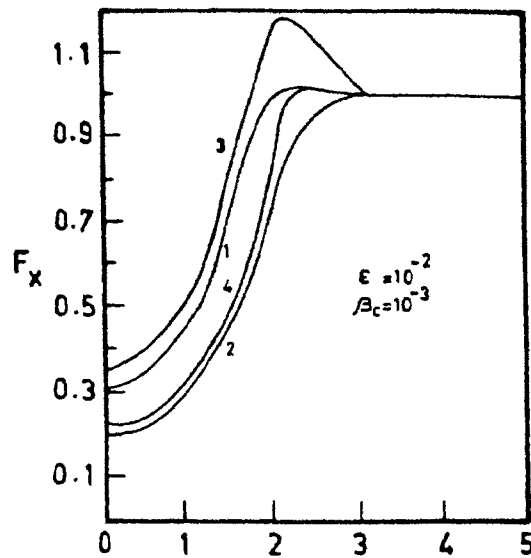


Figure 4:

The ordinate gives relative fluxes for coherent electron scattering with $\epsilon = 10^{-2}$ and $\beta_e = 10^{-3}$. The numbers denote the following cases 1) R_I, R_{II} with $\beta_e = 10^{-2}$ and $T = 155$ 2) R_I, R_{II} with $\beta_e = 10^{-3}$ and $T = 155$ 3) R_I, R_{II} CRD with DAP for $\beta_e = 10^{-2}$ and $T = 5 \times 10^4$ 4) R_I, R_{II} for $\beta_e = 10^{-3}$ and $T = 5 \times 10^4$.

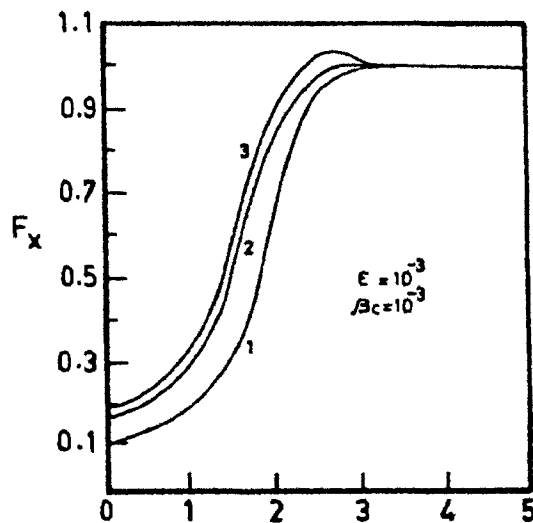


Figure 5

Same as figure 4 with $\epsilon = 10^{-3}$ and $\beta_e = 10^{-3}$. The numbers denote the following cases. 1) R_I, R_{II}, R_{III} with $\beta_e = 10^{-3}$ $T = 155$. 2) R_I, R_{II}, R_{III} with $\beta_e = 10^{-2}$ and $T = 155$, 3) R_I, R_{II} , CRD with VAP for $\beta_e = 10^{-2}$ and $T = 5 \times 10^4$.

very small emission component. These characteristics are reflected in Fig. 4. When the thermal sources are reduced (Fig.5), there are less number of photons to be redistributed into the transition region between core and the wing. Consequently we do not find a substantial emission hump.

3.4.3. Comparison of solutions for different electron scattering coefficients

When the electron scattering coefficient is reduced, the opacity in the wing is reduced and this results in higher absolute flux values in the wing. Absolute flux at line centre will not be affected because of the high line absorption coefficient at the centre. Therefore the relative flux in the core will be more for a larger electron scattering coefficient. Hence we get deeper and broader lines for small β_e 's. Figures 4 and 5 illustrate this result.

3.4.4. Non-coherent electron scattering

The combined effect of various atomic redistribution functions and non-coherent electron scattering on emergent flux profiles is plotted in figures 6-8. The result for DAP (Fig. 6) is in complete agreement with that of Auer and Mihalas (1968). Non-coherent electron scattering combined with PRD by atoms give higher flux values in the core compared to coherent electron scattering for the parameters $T = 5 \times 10^4$,

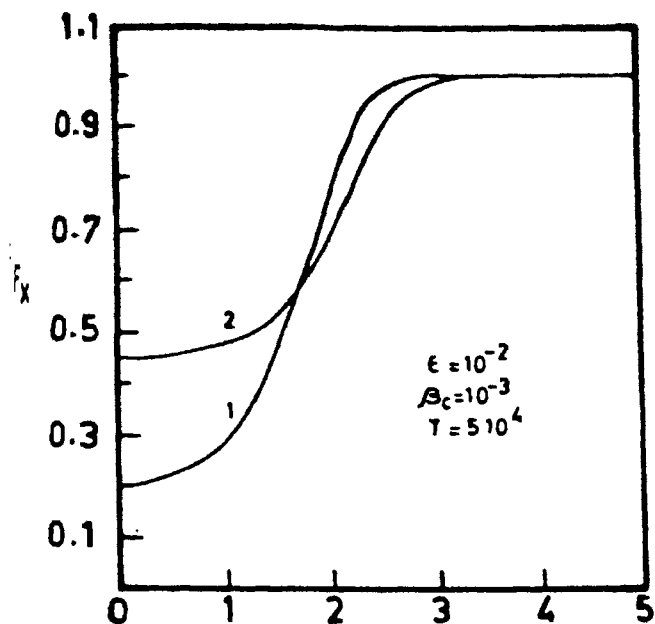


Figure 6: same as fig.4 for non-coherent electron scattering. The numbers denote the following cases: 1) R_I , R_{II} CRD with DAP and VAP for $\beta_e = 10^{-4}$, 2) R_{II} , R_{III} for $\beta_e = 10^{-3}$.

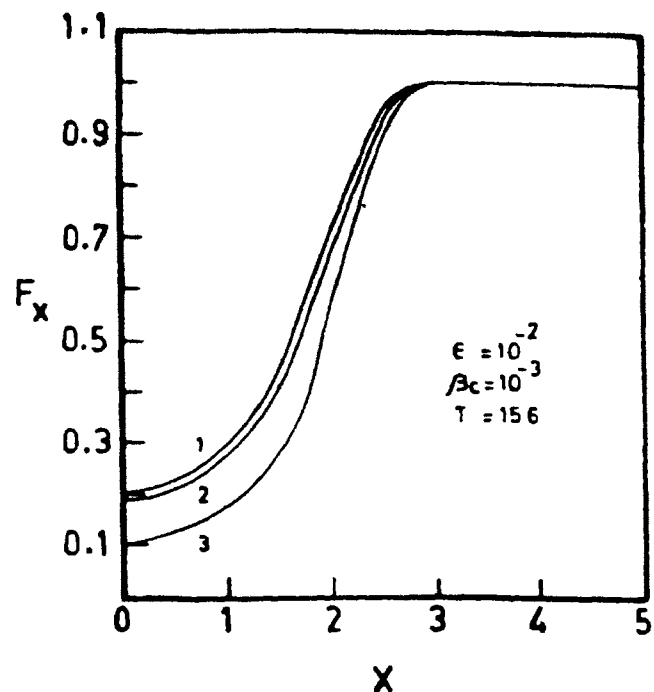


Figure 7: The numbers denote the following cases 1) R_I CRD with DAP, VAP for $\beta_e = 10^{-3}$. 2) R_{II} , CRD with DAP, CRD with VAP for $\beta_e = 10^{-4}$. 3) R_{II} with $\beta_e = 10^{-4}$, $\epsilon = 10^{-3}$.

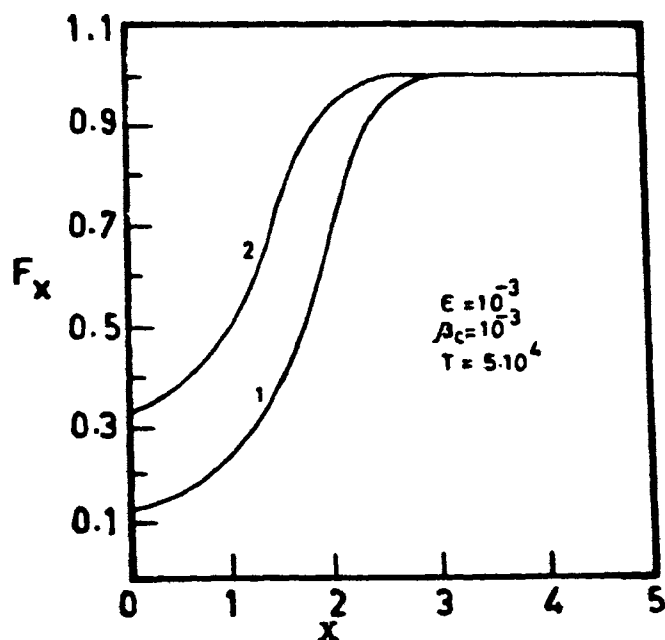


Figure 8: Numbers denote the following cases: 1) R_I , R_{II} , CRD with VAP for $\beta_e = 10^{-3}$ and 2) R_I , R_{II} CRD with DAP and VAP for $\beta_e = 10^{-2}$.

$\epsilon = 10^{-2}$, $\beta_c = 10^{-3}$ and $\beta_e = 10^{-3}$ (Fig 4,6). When ϵ is reduced to 10^{-3} , we find that there is no significant difference between the flux profiles due to coherent and non-coherent electron scatterings. The same result holds good when the total optical depth of the medium is reduced.

CHAPTER 4EFFECT OF EMISSION PROFILE ON LINE FORMATION4.1 Introduction

The emission profile ψ_ν is defined as the fraction of all atoms in the upper state that, if they decay radiatively, emit photons of frequency ν as seen in the laboratory frame (Mihalas, 1978).

For a resonance line photon, we know a priori (i.e. without a dependence on the radiation field and/or level populations) the functional form of the absorption profile. This is due to the inherent assumption of Maxwellian velocity distribution for the atoms in the lower level, which is quite valid in the stellar atmospheric conditions. If the absorption and emission can be regarded as two independent processes, the equality of absorption and emission profiles is assured. If there is any correlation between the absorption and the subsequent emission, we see that the emission profile is dependent on the radiation field. Since such a correlation exists in partial redistribution formalism, we find that the absorption and emission profiles need not be identical. Our aim is to find the deviation between the absorption and emission profiles when the partial redistribution functions are used in radiative transfer calculations.

Oxenius (1965) showed that the emission profile not

only depends on the radiation field, but also on the velocity distributions of the atoms in the ground and excited states. Even though his formalism is physically consistent, is not suitable for numerical calculations. On the other hand, the sub-state formalism of Milkey and Mihalas (1973) enables a quantitative study. Steinitz and Shine (1973) investigated the assumption of the equality of the absorption and emission profiles for a two level atom with Doppler redistribution. Baschek, Mihalas and Oxenius (1981) showed that the formulation given by Mihalas (1978) of the stimulated emission term is incorrect. The error committed in the calculations presented thus far in the literature is of no importance because the stimulated emission term is negligible in all the cases. They gave correct expressions for the statistical equilibrium equations for angle averaged isotropic redistribution functions.

We note that the above expressions are in conformity with that of the equations of Steinitz and Shine (1973). Since we are interested in angle averaged redistribution of the radiation field in the present study, we will closely follow the above formalism. We have obtained the emission profile when the stimulated emission is not negligible. In the case of non-coherent redistribution of the photons, we expect a close equality between absorption and emission profiles. But the opposite case of a redistribution which is highly coherent in the wings is expected to make the absorption and emission

profiles quite different from each other. So, such a situation is studied. In section 4.2, the form of frequency dependent source function and the method of solution are given. Here we shall show the equality of the expressions of Steinitz and Shine (1973) and Baschek, Mihalas and Oxenius (1981) for the source functions. Since the formalism of Steinitz and Shine (1973) enable us to define emission profile in a simple way, we have adopted this method. In section 4.3, we discuss the results briefly.

4.2. The source function including the emission profile.

The transfer equation for a two level atom without continuous absorption can be written as,

$$\mu \frac{dI_\nu}{d\tau_\nu} = \phi_\nu (I_\nu - S_\nu) \quad (4.1)$$

where S_ν can be written as,

$$\begin{aligned} S_\nu &= \frac{2h\nu^3}{c^2} \left[\frac{\omega(\nu)}{\frac{g_2 n_1}{g_1 n_2} - \omega(\nu)} \right] \\ &= \frac{2h\nu^3 / c^2 \left[\frac{g_1 n_2 \psi_\nu}{g_2 n_1 \phi_\nu} \right]}{1 - \frac{g_1 n_2}{g_2 n_1} \frac{\psi_\nu}{\phi_\nu}} \quad (4.2) \end{aligned}$$

where $\omega(\nu) = \psi_\nu / \phi_\nu$, $\psi(\nu)$, $\phi(\nu)$ being the emission and

absorption profiles, n_1 , n_2 are the number densities of the lower and upper levels respectively. The other symbols have their usual meaning. Our aim is to express the number densities by some tractable parameters. The statistical equilibrium equations for a two level atom taking the absorption and emission profiles properly into account become (Baschek et.al , 1981)

$$n_2 \psi_\nu \left[A_{21} + B_{21} \int J_{\nu'} \psi_{\nu'} d\nu' + C_{21} \right] = n_1 \left[B_{12} \int J_{\nu'} R(\nu', \nu) d\nu' + C_{12} \psi_\nu^* \right] \quad (4.3)$$

and

$$n_1 + n_2 = N_{\text{atom}} \quad (4.4)$$

Isotropy, angle averaging, and a near Maxwellian velocity distribution for the atoms in the upper states are the assumptions made in the above equations. The fact that the spontaneous and stimulated emission profiles are same (Dirac, 1958) is also used in arriving at equation (4.3). $R(\nu', \nu)$ is the angle averaged redistribution in the observer's frame. A_{21} , B_{21} and B_{12} are the Einstein spontaneous emission, induced emission and absorption coefficients. Equation (4.3) represents the number of atoms which can emit at frequency ν . The first term in the L.H.S of equation (4.3) represents the number of atoms which emit spontaneously. The integral in the second term accounts for all atoms which can be depleted by induced emissions over all frequencies. C_{21} and C_{12} are the

collisional de-excitation and excitation rates. The first term on the R.H.S of equation (4.3) gives the number of atoms which absorb at frequency ν' and emit at frequency ν . ψ_{ν}^* is the natural excitation profile which is the same as the absorption profile ϕ_{ν} . The absorption profile has been defined in equation (2.9) as the integral over frequency of the redistribution function. Equation (4.4) represents the conservation of atoms. Integrating equation (4.3) over ν we get,

$$n_2 \left[A_{21} + B_{21} \int J_{\nu} \psi_{\nu} d\nu' + C_{21} \right] = n_1 \left[B_{12} \int J_{\nu} \phi_{\nu} d\nu' + C_{12} \right] \quad (4.5)$$

Defining,

$$\int J_{\nu} \psi_{\nu} d\nu' = J_e \quad ; \quad \int J_{\nu} R(\nu', \nu) d\nu' = J_R$$

and

$$\int J_{\nu} \phi_{\nu} d\nu' = J_a \quad (4.6)$$

we get from the equation (4.3) the following relation :

$$\frac{n_2 \psi_{\nu}}{n_1 \phi_{\nu}} = \frac{B_{12} J_R \phi_{\nu}^{-1} + C_{12}}{A_{21} + B_{21} J_e + C_{21}} \quad (4.7)$$

Using the Einstein relations,

$$A_{21} = \frac{2h\nu^3}{c^2} B_{21} \quad ; \quad B_{12} = \frac{g_2}{g_1} B_{21}$$

and the thermodynamic relations,

$$\frac{C_{12}}{C_{21}} = \left[\frac{n_2}{n_1} \right]^* = \frac{g_2}{g_1} e^{-\frac{h\nu}{kT}} ; B_{\nu} = \frac{2h\nu^3}{c^2} \frac{1}{e^{\frac{h\nu}{kT}} - 1}$$

we get the numerator of the equation (4.2) as

$$A_{21} \left[J_a \phi_{\nu}^{-1} + e' B_{\nu} \right] / A_{21} + B_{21} J_e + C_{21} \quad (4.8)$$

where
$$e' = \frac{C_{21}}{A_{21}} \left[1 - e^{-\frac{h\nu}{kT}} \right]$$

From equation 4.5 we get,

$$\frac{n_2}{n_1} = \frac{A_{21} + B_{21} J_e + C_{21}}{B_{12} J_a + C_{12}} \quad (4.9)$$

Using equation (4.9) and the definition of ω_{ν} we get the denominator of equation (4.2) as,

$$\frac{A_{21} + B_{21} \left[J_e - \omega_{\nu} J_a \right] + C_{21} \left[1 - \omega_{\nu} e^{-\frac{h\nu}{kT}} \right]}{A_{21} + B_{21} J_e + C_{21}} \quad (4.10)$$

Dividing equation (4.8) by equation (4.10) we get,

$$S_{\nu} = \xi_{\nu} \left[J_a \phi_{\nu}^{-1} + e' B \right] \quad (4.11)$$

where
$$\xi_{\nu} = \left[1 + \frac{B_{21}}{A_{21}} (J_e - \omega_{\nu} J_a) + \frac{C_{21}}{A_{21}} (1 - \omega_{\nu} e^{-\frac{h\nu}{kT}}) \right]^{-1}$$

Equation (4.11) was obtained by Baschek, Mihalas and Oxenius (1981). We shall show below that the expression used by Steinitz and Shine (1973) is the same as equation (4.11) for the source function.

4.2.1. Steinitz and Shine formalism

Steinitz and Shine (1973) assumed the emission profile to consist of scattering and collisional parts. The usual assumption of the equality between the emission profile due to collisional transitions and the absorption profile is made. Therefore,

$$\psi_{\text{coll}}(\nu) = \phi(\nu). \quad (4.12)$$

For frequency dependent light, the probability per. absorption is,

$$\frac{J(\nu')R(\nu',\nu)}{J_a} \quad (4.13)$$

J_a is the normalization factor as defined in equation (4.6). Integrating the equation (4.13) over the initial states ν' , we get the frequency dependence of the scattering.

$$\psi_{\text{scatt}}(\nu) = \frac{J_s(\nu)}{J_a} \quad (4.14)$$

Finally the emission profile is defined as the weighted mean of the collisional emission and scattering emission profiles:

$$\psi(\nu) = \frac{J_a + \epsilon' B_\nu \phi(\nu)}{J_a + \epsilon' B_\nu} \quad (4.15)$$

$\frac{n_2}{n_1}$ ratio is obtained from equation (4.5). Substituting $\frac{n_2}{n_1}$ ratio and the definition of ψ_ν in equation (4.2) we obtain an alternative form for S_ν . Now S_ν is given by,

$$S_\nu = \frac{J_a / \phi_\nu + \epsilon' B_\nu}{1 + \epsilon' + \frac{1}{\sigma} E(\nu)} \quad (4.16)$$

where

$$\sigma = \frac{2h\nu^3}{c^2} \quad (4.17)$$

and

$$E(\nu) = \omega(\nu) \int J_{\nu'} \phi_{\nu'} \left[\frac{\omega_{\nu'}}{\omega_\nu} - 1 \right] d\nu' + \epsilon' B_\nu [1 - \omega_\nu] \quad (4.18)$$

Equation (4.16) was derived by Steinitz and Shine (1973).

4.2.2 Equality of equation (4.16) and equation (4.11).

Substituting equation (4.18) into equation (4.16) we get,

$$\begin{aligned}
S(\nu) &= \frac{J_{\mathbf{R}} \phi_{\nu}^{-1} + \epsilon' B_{\nu}}{1 + \epsilon' + \frac{1}{\sigma} \left[\omega_{\nu} \int J_{\nu'} \phi_{\nu'} \left(\frac{\omega_{\nu'}}{\omega_{\nu}} - 1 \right) d\nu' + \epsilon' B_{\nu} (1 - \omega_{\nu}) \right]} \\
&= \frac{J_{\mathbf{R}} \phi_{\nu}^{-1} + \epsilon' B_{\nu}}{1 + \frac{B_{21}}{A_{21}} (J_e - \omega_{\nu} J_a) + \frac{C_{21}}{A_{21}} (1 - e^{-h\nu/kT}) \left(1 + \frac{1}{e^{h\nu/kT} - 1} - \frac{\omega_{\nu}}{e^{h\nu/kT} - 1} \right)} \\
&= \frac{J_{\mathbf{R}} \phi_{\nu}^{-1} + \epsilon' B_{\nu}}{1 + \frac{B_{21}}{A_{21}} (J_e - \omega_{\nu} J_a) + \frac{C_{21}}{A_{21}} (1 - \omega_{\nu} e^{-h\nu/kT})} \quad (4.19)
\end{aligned}$$

Now we see that equation (4.19) is the same as equation (4.11)

Equation (4.19) reduces to the correct form for CRD when we assume $\psi_{\nu} = \phi_{\nu}$.

From equation (4.16) we get,

$$S_{\nu} = \frac{\frac{j_{\mathbf{R}}}{\phi_{\nu}} + \epsilon' B_{\nu}}{1 + \epsilon' + \rho \left(\frac{E}{B} \right)} \quad (4.20)$$

where

$$\rho = \frac{B}{\sigma} = \left[e^{h\nu/kT} - 1 \right]^{-1} ; B_{\nu} \equiv B ; j_{\mathbf{R}} = J_{\mathbf{R}} / B \quad (4.21)$$

We use the equation (4.20) for the source function along with the definition of emission profile given by equation (4.15).

These definitions make it easier to evaluate the emission profile and this formalism is very suitable for studying parametrized models in which we are interested.

4.2.3. Definition of optical depth.

The optical depth for a simple two level atom is given by,

$$d\tau_\nu = -\frac{h\nu_0}{4\pi} \left[n_1 B_{12} \phi_\nu - n_2 B_{21} \psi_\nu \right] dz \quad (4.22)$$

Defining

$$j_a = \frac{J_a}{B} \quad \text{and} \quad j_e = \frac{J_e}{B} \quad (4.23)$$

and using equation (4.5) we obtain,

$$d\tau_\nu = \Delta\tau_\nu \left[1 - \frac{\rho (j_a + e') \omega_\nu}{1 + \rho j_e + e' (1+\rho)} \right] \quad (4.24)$$

where

$$\Delta\tau_\nu = -\frac{h\nu_0}{4\pi} n_1 B_{12} \phi_\nu \Delta z \quad (4.25)$$

4.2.4. The procedure for solving the transfer equation.

We do not know J_e a priori and so we employ an iteration procedure to obtain the emission profile and the radiation field consistently. The total optical depth at the line centre is fixed as $2000 \sqrt{\pi}$. Using this optical depth

scale and the CRD source function, the transfer equation is solved in plane parallel geometry using Feraiah's code. Having known the radiation field, we use it in the definitions of ψ_ν , J_e , J_a and J_x to obtain these quantities. New optical depth scales can be constructed from equation (4.24). The line centre optical depth remains more or less the same because ω_ν at the line centre is almost unity. Now we use equation (4.20) for source function. With these definitions for source function and optical depth scale we solve the transfer equation once again to determine the new emission profile and the radiation field. This iteration procedure is continued till we reach a 1% agreement for the emission profile and the radiation field between any two successive iteration values. It takes normally 5 iterations for $\rho=2.0$ and 3 iterations for $\rho=0.2$.

We see that the parameter ρ gives the measure of the importance of stimulated emission. When $\rho > 1$, the stimulated emission is important. We have used the values 2.0 and 0.2 for ρ . ϵ' is assumed to be 10^{-3} . This fixes the contribution from the thermal sources. When ρ is high i.e. when stimulated emission term is dominant term, the procedure outlined is unsuitable for solving the problem. Linearization technique given by Milkey and Mihalas (1973) is probably more appropriate in these situations. When the ρ is increased to 5 it requires a large number of iterations and a convergent solution is difficult to obtain.

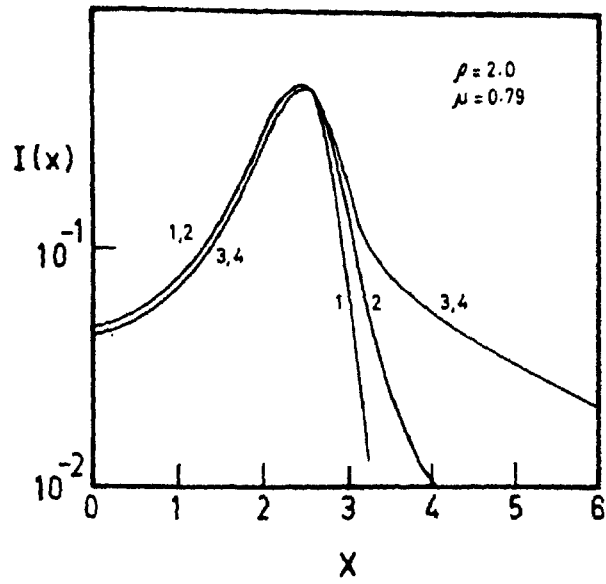


Figure 1 Emergent intensity at $\mu = 0.79$ with $\rho = 2.0$. The numbers denote the following cases. (1) R_I (2) R_{II} (3) R_{III} (4) CRD with VAP.

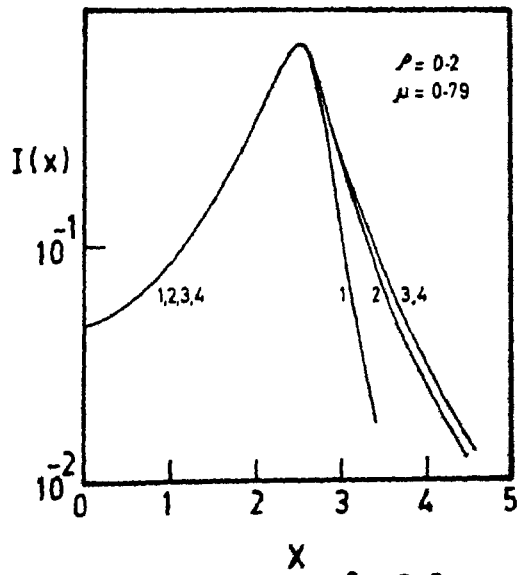


figure 2 same as fig.1 with $\rho = 0.2$

24 frequencies and 2 angles are employed. The frequency grid is chosen as $x = (0,6)$ where x is measured in Doppler units. Necessary modifications are made in Peraiah's code to solve this particular problem.

4.3. Results and discussion.

We considered a medium with pure thermal sources and no incident radiation. E_{ν} is set equal to 1. In Fig. 1 we have plotted the final emergent intensities at $\mu = 0.78$ for several redistribution functions and for $\rho = 2.0$. The result for R_I agrees with that of Steinitz and Shine. Though in the core, all the different redistribution functions give the same intensity, we see large differences in the wing. The emergent intensity due to R_{III} function closely matches with that of CRD. Even an enhanced stimulated emission does not make the emergent intensity due to R_{III} deviate from CRD. Fig. 2 gives the final emergent intensities at $\mu = 0.78$ for R_I , R_{II} and R_{III} for $\rho = 0.2$. Now we have reduced the contribution from stimulated emission term. These cases require fewer iterations for convergence. Now we see that the absorption in the core is strengthened and also the differences between the emergent intensities due to various redistribution functions in the wing is also reduced. So the stimulated emission enhances the differences between various redistribution functions and hence the emission profile differs more from absorption profile. This result is illustrated in the next

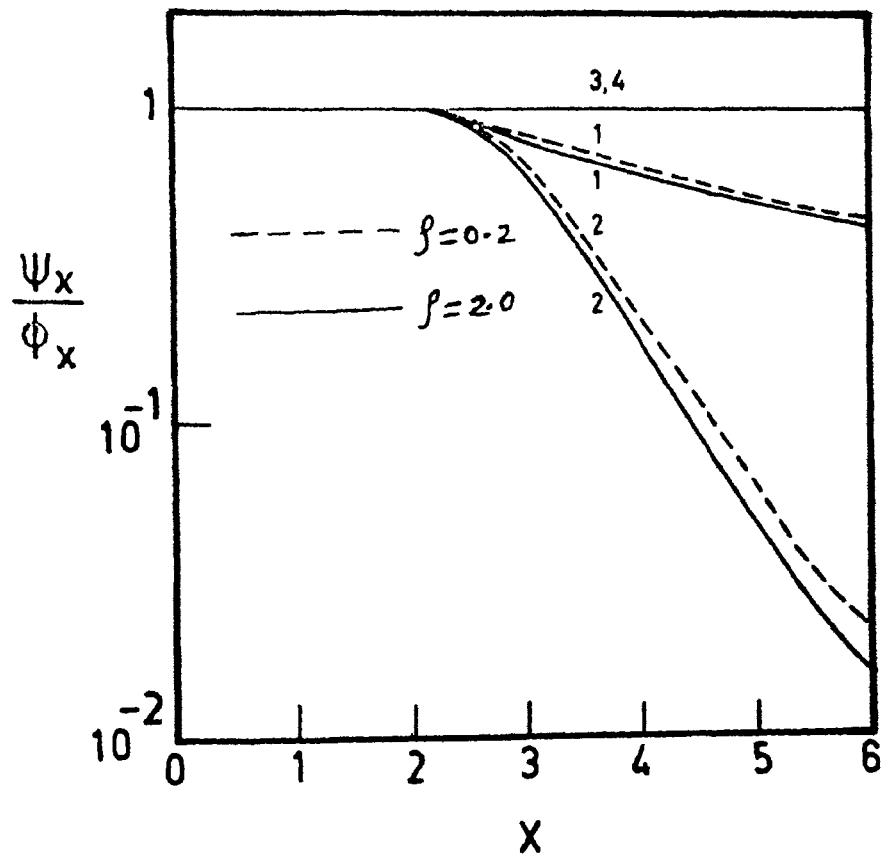


Figure 3 Ratio of emission to absorption profiles at $\tau \approx 0$. (1) R_I (2) R_{II} (3) R_{III} (4) CRD with VAP.

figure. In Fig. 3 we have plotted the ratio of emission to absorption profiles at the outermost shell of the medium for $\rho = 2.0$ and 0.2 . CRD gives the ratio of 1 throughout the medium which is as it should be. This acts as a check for our numerical computations. R_{III} function gives a ratio which is very close to 1. Even though $R_{\text{III}} \neq \phi(x')\phi(x)$ in the wings (Finn, 1967), the non coherency makes the ratio ψ_{ν} / ϕ_{ν} to be almost 1. This result seems to hold good for the extreme situations which we have considered and so may be quite general. The coherency in the wing for R_{II} make the photons to be emitted selectively in the wings. This makes the ratio ψ_{ν} / ϕ_{ν} to be quite different from 1. R_{I} is less coherent than R_{II} in the wings (see Fig. 5, chapter 2) and so this ratio does not deviate from 1 as much as for R_{II} . This ratio is closer to 1 when the contribution from the stimulated emission is reduced.

In the core, for all the cases we see that ψ_{ν} / ϕ_{ν} does not deviate from 1 even if the stimulated emission term is important. We can conclude that in the Doppler core, one can approximate the redistribution functions to CRD and for all practical purposes, one can approximate R_{III} by CRD with Voigt absorption profile even when we formulate the transfer equation taking into account the difference between absorption and emission profiles.

CHAPTER 5
EFFECT OF SMALL MACROSCOPIC VELOCITIES ON
Ca II H AND K LINES

5.1. Introduction

Linsky and Avrett (1970) reviewed theoretical and observational studies of the profiles of Ca II H and K and infrared triplet lines in the sun, which included some of their calculations. They took five levels plus continuum as their atomic model to represent Ca II ion. Integral equation approach was used for the calculation of line source function. Complete redistribution was assumed in their computations. Shine, Milkey and Mihalas (1975) studied the effect of partial frequency redistribution on the formation of Ca II H and K lines in the solar atmosphere. They found the PRD results to be in better agreement with the observations. The calculations described above are based on a static atmosphere. Consequently the computed profiles were symmetric.

Asymmetric profiles with a single peak emission of the K lines were observed at high spatial resolution studies (Pasachoff, 1970). To account for the asymmetric profile, Athay (1970) assumed velocity fields in the regions of line formation. He concluded that to obtain K_{2v} enhancement, either the layers where K_2 is formed are moving upward with velocities of $3-7 \text{ km s}^{-1}$ or the K_2 layers are moving downward

with velocities of $10-20 \text{ km s}^{-1}$ but he tends to favour the second alternative. He assumed a three level atom model with continuum. He used the integral equation technique generalized for a multi level atom. Basri, Linsky and Eriksson (1981) used a comoving partial frequency redistribution code to model the outer atmospheres of cool type stars. They obtained a highly asymmetric profile of Ca II K line which agrees with the observation of this line in β Dra.

Line formation in moving media was studied by Abhyankar (1964) and Kulander (1968). Peraiah (1978) gave an algorithm for solving the transfer equation including velocity fields in spherically symmetric expanding media. Rangarajan, Mohan Rao and Peraiah (1981) investigated the effect of velocities of the order of 2 km s^{-1} and 4 km s^{-1} in an expanding atmosphere with chromospheric type of temperature increase.

This chapter is based on the above work. Here we present the profiles of Ca II H & K (3968A, 3933A) and infrared triplet lines (8489A, 8662A and 8542A) formed in slowly expanding media. Five levels with continuum is taken as the atomic model. The formalism of Grant and Peraiah (1972) for the two level atom model is extended to include multi level atom model. Transfer equation is solved in observer's rest frame using Peraiah's code (1978). Profiles are computed for systematic expanding velocities, $v = 0.5$ and 1.0 (expressed in mean thermal units) Profiles calculated in static media

($v = 0.0$) are also shown for comparison purposes. Since we have not incorporated a realistic atmospheric model with micro-turbulent velocities and continuous absorption, we can not compare our results with observations directly. Nevertheless the study underlines the importance of velocities in determining the shapes of lines. This study also demonstrates the easy extension of Discrete space theory technique to solve transfer equation when a number of physical processes are included. In section 5.2, we give the atomic model chosen and the method of calculation of various rates. We discuss the computational procedure in section 5.3. Section 5.4 contains the results.

5.2. Atomic model

Atomic model chosen is represented in Fig. 1. We have taken the $4^2S_{1/2}$ ground level, $4^2P_{1/2}$ and $4^2P_{3/2}$ upper levels, $3^2D_{3/2}$ and $3^2D_{5/2}$ metastable levels and the continuum. Temperature (T_e) and the electron number density (n_e) distributions for our atmosphere are given in figures (2) and (3).

Collisional and radiative excitational and de-excitational processes are considered. Photoionization, photo-recombination, collisional ionization and recombination between the continuum and all the levels are also included.

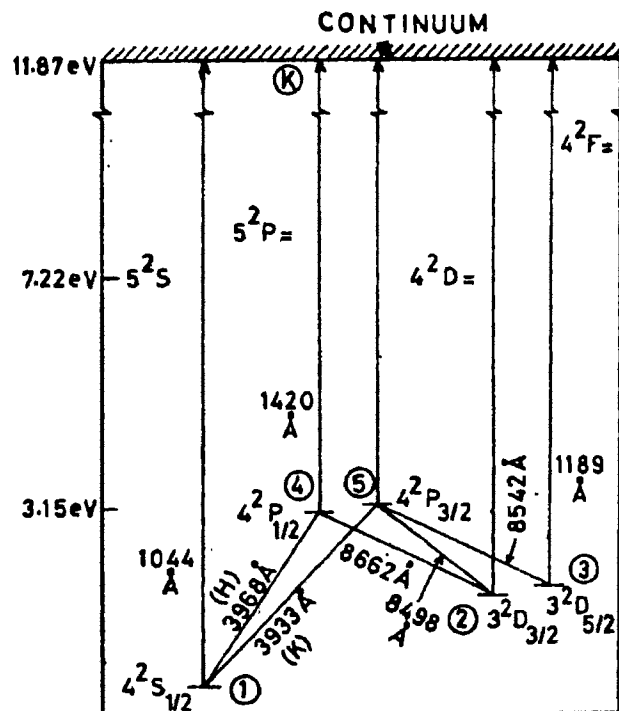


Figure 1. Energy level diagram for CaII ion with the permitted radiative transitions.

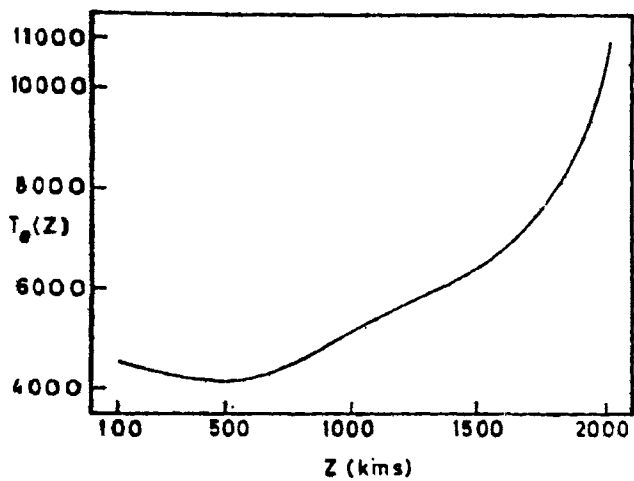


Figure 2 Temperature T_e ($^{\circ}$ K) distribution of the model chosen is given against the height Z (kms) in the atmosphere.

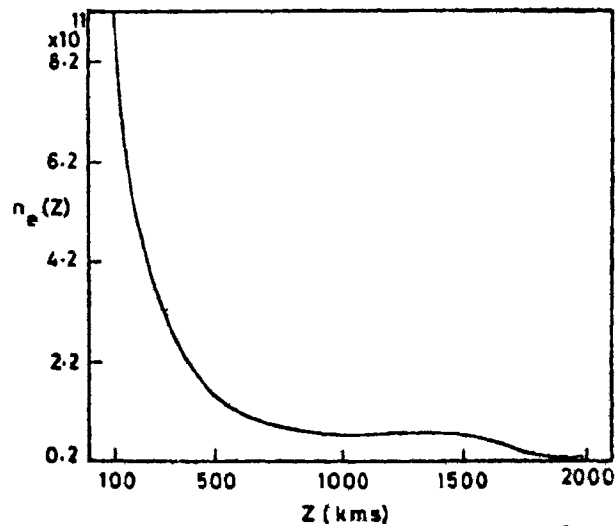


Figure 3 Electron number density n_e (per cubic cm) is given with respect to the height Z (kms) in the atmosphere.

Photoionization rates are calculated according to the formula

$$R_{ik} = 4\pi \int_{\nu_i}^{\infty} \frac{d\nu}{h\nu} \alpha_i(\nu) J_\nu(z) \quad (5.1)$$

i denotes the lower level and k refers to the continuum. z is the height of the atmospheric layer. We approximate $J_\nu(z) = B_\nu(z)$ where $B_\nu(z)$ is the Planck function. $\alpha_i(\nu)$ is the photoionization cross section and is taken from Peach's tables (1967). Recombination rates follow from the detailed balance arguments and they are given by

$$R_{ki} = \left[\frac{n_i}{n_k} \right]^* R_{ik} \quad (5.2)$$

where $\left[\frac{n_i}{n_k} \right]^*$ is the LTE (Local Thermodynamic Equilibrium) population density ratio obtained from Saha-Boltzmann relation.

Collisional recombination rates are calculated from the formula given in Linsky's Ph.D. thesis (1969) with the corrections for the inclusion of both the D levels. Detailed balance arguments give the collisional ionization rates by the formula

$$C_{ik} = C_{ki} \left(\frac{n_k}{n_i} \right)^* \quad (5.3)$$

Spontaneous emission rates (Einstein A values) between the bound levels are taken from the Wiese tables (1969). Collisional excitation and de-excitation rates are calculated according to Giovanelli (1967). Multiplet relations are used to get rates for the sub-levels. To calculate the fine structure transition rates $C(4^2P_{3/2} - 4^2P_{1/2})$ and $C(3^2D_{3/2} - 3^2D_{1/2})$, Dumont's (1967) cross sections are used and they are derived by treating the collisions to be elastic and collisions with protons to be dominant.

5.3. Computational procedure

The transfer equation which we have considered is

$$\mu \frac{dI(x, \mu, z)}{dz} = k_L(z) \phi(x, \mu, z) \left[S(x, z) - I(x, \mu, z) \right] \quad (5.4)$$

and for the oppositely directed beam

$$-\mu \frac{dI(x, -\mu, z)}{dz} = k_L(z) \phi(x, -\mu, z) \left[S(x, z) - I(x, -\mu, z) \right] \quad (5.5)$$

where the symbols have been described in earlier chapters. Now we see that the profile function becomes angle dependent.

The equations (5.4) and (5.5) are transformed into the optical depth scale where

$$d\tau = -k_L(z)dz = \frac{h\nu_0}{4\pi\Delta\nu_D} \left[n_l(z)B_{lu} - n_u(z)B_{ul} \right] dz \quad (5.6)$$

B_{lu} and B_{ul} are the Einstein absorption and induced emission coefficients for the transition between the lower level (l) and the upper level (u). n_l and n_u are the number densities of the lower and upper levels of the transition. ν_0 is the line centre frequency. $\Delta\nu_D$ is the Doppler width defined as

$$\Delta\nu_D = \frac{\nu_0}{c} \left(\frac{2kT}{m} \right)^{1/2} \quad (5.7)$$

The profile function $\phi(x, \mu, z)$ is defined by

$$\phi(x, \mu, z) \equiv \bar{\phi}(x - \mu v, z) \quad (5.8)$$

where $x = (\nu - \nu_0) / \Delta\nu_D$ and v is the velocity measured in mean thermal units. When there is velocity field, the frequency of the line photon is shifted by

$$x' = x - \mu v(\tau) \quad (5.9)$$

$v(\tau)$ is the velocity at the point τ .

We have used complete redistribution with Voigt profile function $H(\alpha, x)$. Damping parameter ' α ' is assumed to be 10^{-3} throughout the medium. The formulation of multilevel transfer problem using PRD type of scattering mechanism in the presence of velocity fields is yet to be completed within the framework

of Discrete space theory technique. Complete linearization method is probably an ideal setup for the above mentioned formulation. When we attempted this task, we found that we need to have fast computers to get the results, because of the requirement of large memory to store the matrices. Since at present we do not have access to such machines, here we present only CRD results which we could do within our available resources.

The statistical equilibrium equations for a multi-level atom are given by

$$n_i \left[\sum_{j>i} (B_{ij} \bar{J}_{ij} + C_{ij}) + R_{ik} + C_{ik} + \sum_{j<i} (A_{ij} + B_{ij} \bar{J}_{ij} + C_{ij}) \right] \\ = \sum_{j>i} n_j (A_{ji} + B_{ji} \bar{J}_{ij} + C_{ji}) + \sum_{j<i} n_j (B_{ji} \bar{J}_{ij} + C_{ji}) + n_k (R_{ki} + C_{ki}) \quad (5.10)$$

In the above expression, the radiative transitions are significant only for permitted transitions. \bar{J} is defined in equation (5.17).

$$\sum_{i=1}^M n_i + n_k = N_{Ca^+} \quad (5.11)$$

where N_{Ca^+} is the number of Ca^+ ions and M is the number of levels considered. N_{Ca^+} at the outermost shell is chosen to be 10^7 and the number density in the medium is varied according to the equation of continuity. We divided the medium into 5 shells.

We have employed equivalent two level atom approach to write the expression for the source function (Mihalas, 1978). Consider a line formed between levels l and u . The line source function is given by

$$S_{lu} = \frac{2h\nu_o^3}{c^2} \frac{n_u}{\frac{g_u}{g_l} n_l - n_u} = \frac{2h\nu_o^3}{c^2} \frac{1}{\frac{g_u n_l}{g_l n_u} - 1} \quad (5.12)$$

The rate equation for the lower level in a multi level environment is

$$\begin{aligned} n_l (B_{lu} \int \phi_\nu J_\nu d\nu + C_{lu} + \sum_{i < l} A_{li} Z_{li} + \sum_{l < j \neq u} C_{lj} Y_{lj} + R_{lk} + C_{lk}) \\ - n_u (A_{ul} + B_{ul} \int \phi_\nu J_\nu d\nu + C_{ul}) = n_l^* (R_{kl} + C_{lk}) \\ + \sum_{l < j \neq u} n_j A_{jl} Z_{jl} + \sum_{i < l} n_i C_{il} Y_{il} \end{aligned} \quad (5.13)$$

and for the upper level we have

$$\begin{aligned} n_u (B_{ul} \int \phi_\nu J_\nu d\nu + C_{ul} + \sum_{u > i \neq l, j} A_{ui} Z_{ui} + \sum_{u < j} C_{uj} Y_{uj} + R_{uk} + C_{uk} + A_{ul}) \\ - n_l (B_{lu} \int \phi_\nu J_\nu d\nu + C_{lu}) = n_u^* (R_{ku} + C_{uk}) + \sum_{u < j} n_j A_{ju} Z_{ju} \\ + \sum_{u > i \neq l} n_i C_{iu} Y_{iu} \end{aligned} \quad (5.14)$$

where the quantities with * as superscripts denote the LTE values. Z_{ji} and Y_{ij} are the net radiative and collisional

brackets defined by

$$Z_{ji} = 1 - \bar{J}_{ij} (n_i B_{ij} - n_j B_{ji}) / n_j A_{ji} \equiv 1 - (\bar{J}_{ij} / S_{ij}) \quad (5.15)$$

and

$$Y_{ij} = 1 - \frac{n_j c_{ji}}{n_i c_{ij}} \quad (5.16)$$

where

$$\bar{J}_{ij} = \int \phi_\nu J_{ij}(\nu) d\nu \quad (5.17)$$

If we eliminate analytically the population ratio appearing in the expression for source function we get

$$S_{lu} = \left[\int_0^\infty \int_{-1}^1 \phi(\nu) I(\nu, \mu, z) d\mu d\nu + (\epsilon' + \theta) B_\nu(T_e) \right] / (1 + \epsilon' + \eta) \quad (5.18)$$

$\epsilon' B_\nu$ is the thermal source term which represents photons that are created by collisional excitation followed by radiative de-excitation. ν is measured from the line centre. The term ϵ' in the denominator is the sink term that represents those photons that are destroyed by collisional de-excitation following a photoexcitation for strong resonance lines like Ca II H and K. ϵ' is given by

$$\epsilon' = C_{ul} (1 - e^{-h\nu/kT}) / A_{ul} \quad (5.19)$$

The effects of radiation field due to other lines are described by terms η and θ . They are expressed as

$$\eta = \left[a_2 a_3 - \left(\frac{g_l}{g_u} \right) a_1 a_4 \right] / \left[A_{ul} (a_2 + a_4) \right] \quad (5.20)$$

and

$$\theta = \left[n_l^* a_1 a_4 (1 - e^{-h\nu/kT}) \right] / \left[n_u^* A_{ul} (a_2 + a_4) \right] \quad (5.21)$$

where in turn,

$$a_1 = R_{lk} + C_{lk} + \sum_{i < l} A_{li} Z_{li} + \sum_{l < j \neq u} C_{lj} Y_{lj} \quad (5.22)$$

$$a_2 = n_l^* (R_{kl} + C_{lk}) + \sum_{l < j \neq u} n_j A_{jl} Z_{jl} + \sum_{i < l} n_i C_{il} Y_{il} \quad (5.23)$$

$$a_3 = R_{uk} + C_{uk} + \sum_{u > i \neq l} A_{ui} Z_{ui} + \sum_{u < j} C_{uj} Y_{uj} \quad (5.24)$$

$$a_4 = n_u^* (R_{ku} + C_{uk}) + \sum_{u < j} n_j A_{ju} Z_{ju} + \sum_{u > i \neq l} n_i C_{iu} Y_{iu} \quad (5.25)$$

Velocity at each shell is given by

$$V(n) = V(A) + \left[\frac{V(B) - V(A)}{N} \right] * n \quad (5.26)$$

where A,B are the inner and outer boundaries of the atmosphere. n denotes the number of the shell and N is the total number of layers. Velocity is measured in thermal Doppler units. We have set $V(A) = 0$ and $V(B) = 0, 0.5$ and 1 . Equations (5.4), (5.5) and (5.10) are solved with the following boundary conditions:

The incident radiation at the top of the atmosphere is zero. The incident radiation at the lower boundary of the atmosphere is assumed to be $B_{\nu}(T_e = 4620^{\circ}\text{k})$.

The above equations are solved iteratively. The LTE number densities are chosen to be initial values for calculating the optical depths from the relation (5.6). To calculate the radiation field in any line, ϕ and η have to be specified, which depend upon the radiation field of other lines. To compute H line radiation field, the radiation field in other lines are assumed to be Planckian. While computing the K line, we substitute the computed H line intensities, keeping the unknown radiation fields in infrared triplet lines as Planckian. This procedure is continued till the intensities of all the five lines are calculated.

To get the number densities in the levels, we substitute the mean intensities of all the five lines in the statistical equilibrium equations. This new number densities are used to calculate the optical depth. Since we know the radiation field in all the lines, we substitute those values to compute the net radiative brackets which are used in the source function expression. Iterations are continued till the number densities converged upto a deviation of less than 1% of the previous iteration values.

5.4. Results

Emergent intensities of K line for the various velocities when $\mu = 0.79$ are plotted in figure 4. The total optical depth at the line centre with the chosen atmospheric model is 618. We find a symmetric profile with a double peaked emission for the static case, and for non-zero velocities, we find blue shift and asymmetry in the profiles. When the velocity at the outer boundary is one mean thermal unit, only a single peak in the red side (K_{2r}) with a blue shift of K_s minimum is obtained. K_s absorption features broaden with velocities. A similar trend is seen in the limb ($\mu = 0.21$) also (Fig. 5). We also find K_{2r} is slightly higher than K_{2v} when $V = 0.5$. Emergent intensities of H line at $\mu = 0.79$ for various velocities are plotted in Fig. 6. H line intensities are consistently higher than than K line intensities. This is due to the lesser optical depth of H line which is only 322 in our model. Both H and K lines exhibit similar trends. Narrow emission peaks occur for $V = 0.5$. Emergent intensities of 8662 line for $\mu = 0.79$ and 0.21 are given in figures 8 and 9. Figures 10 and 11 show the emergent intensities of the line 8542 for $\mu = 0.79$ and 0.21 respectively. Emergent intensity profiles of 8498 are plotted in figures 12 and 13.

All the infrared triplet lines are in absorption except for 8498 line at $\mu = 0.79$. This line is the weakest due to the least optical depth at the line centre. With velocities, we

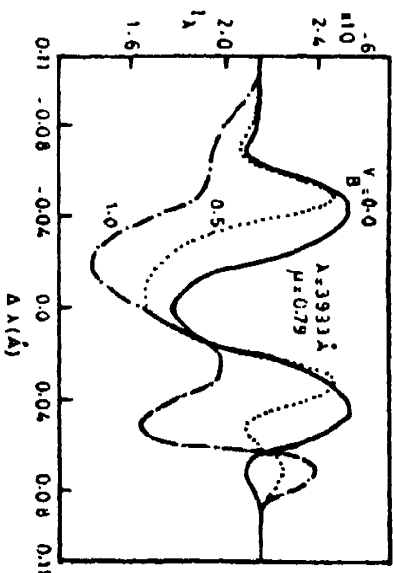


Figure 4 Ordinate: emergent intensity I_λ (ergs cm^{-2} sec^{-1}) of K line (3933 Å) for $\mu = 0.79$ and velocity $V = 0.0, 0.5$ and 1.0 . Abscissa: Displacement $\Delta\lambda$ from the line centre in Å.

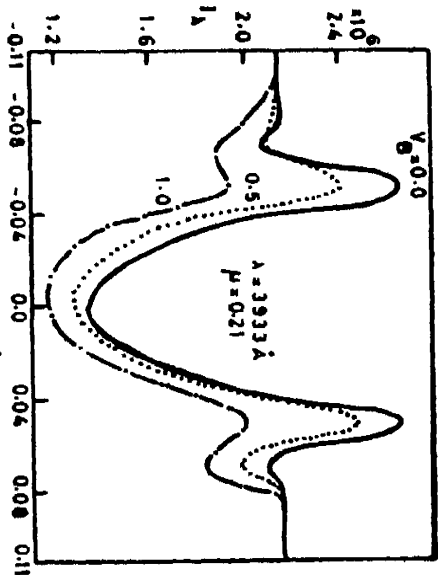


Figure 5. Same as that in Fig. 4 with $\mu = 0.21$.

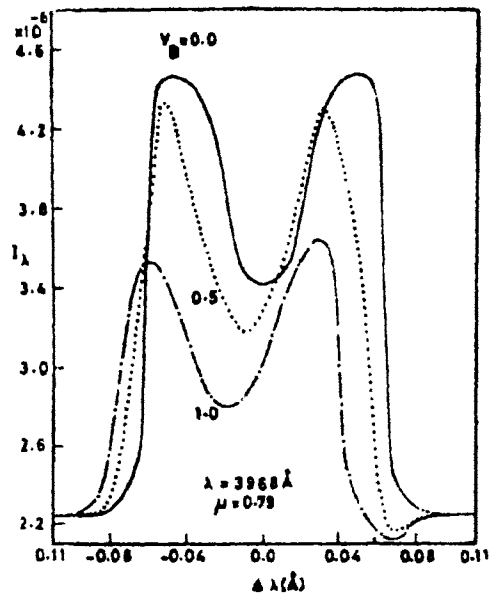


Figure 6 Same as in fig.4 for H line (3968 Å).

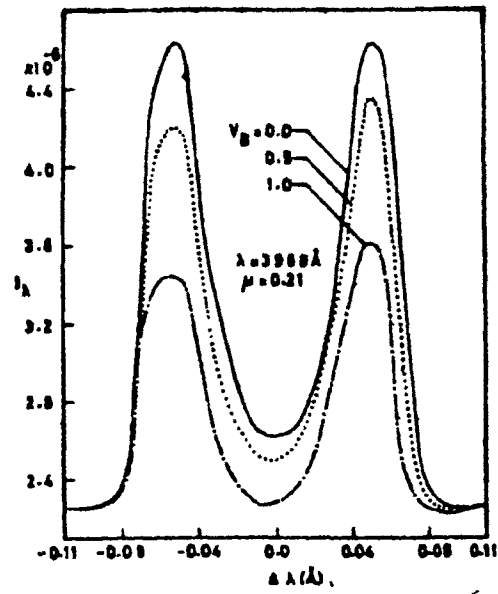


Figure 7 Same as in fig 6 with $\mu = 0.21$.

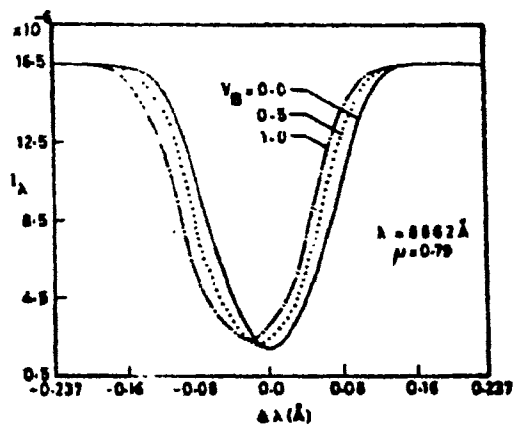


Figure 8 same as in fig.4 for the infrared triplet line 8662 Å.

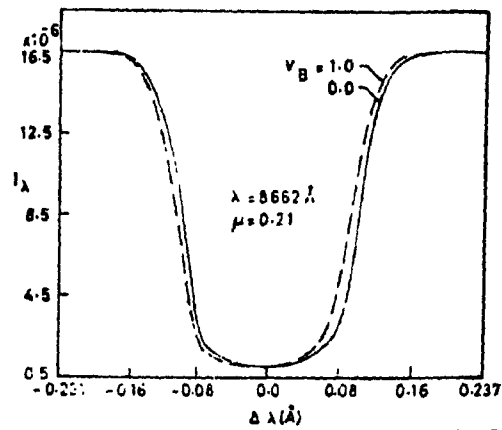


Figure 9 same as in fig.8 with $\mu=0.21$ and for velocities $V_B = 0.0$ and 1.0 only.

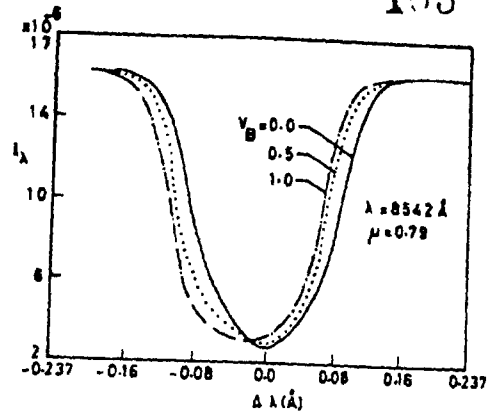


Figure 10 same as in fig.8 for 8542 A.

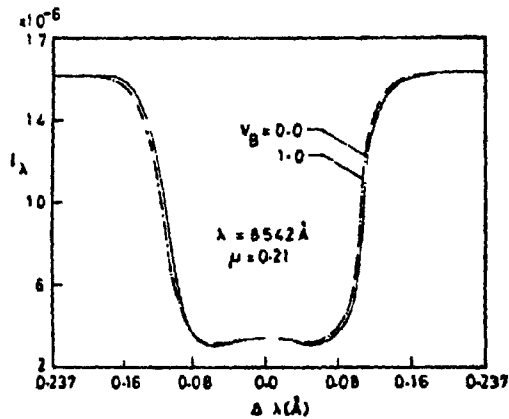


Figure 11 same as in fig.10 with $\mu = 0.21$ and for $V_B = 0.0, 1.0$.

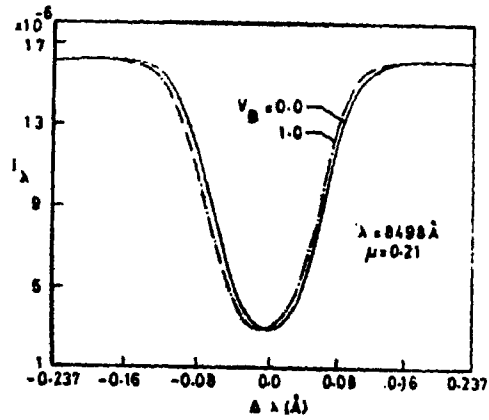


Figure 13 same as in fig.12 with $\mu = 0.21$ and for $V_B = 0.0, 1.0$ only.

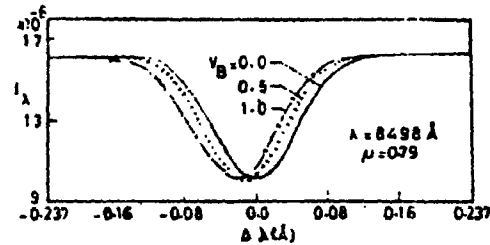


Figure 12 same as in fig.8 for 8498 A line.

find all lines to be blue shifted. Near the limb, the velocity effects in the line profiles are negligible.

CHAPTER 6

CONCLUSIONS AND FUTURE WORK

6.1. Summary of the results.

In this chapter we are stating the results of our study briefly. These results have been illustrated by figures and explained in detail separately in each chapter of this thesis. Some of these results have been in quantitative agreement with that of other workers wherever such comparisons are possible.

We find that the redistribution functions affect the spectral line formation and the extent of the effects depend on the boundary conditions, optical thickness at the line centre and the scattering properties of the medium. From the various schematic line formation problems with different types of redistribution functions which we have studied, we come to a conclusion that the degree of coherency in the wings which the particular type of redistribution exhibits determines the transfer of radiation in strong resonance lines. Therefore the partial redistribution effects have to be taken into account when studying such lines. For the optically thin lines when the continuous absorption is present the redistribution effects are negligible. The presence of continuous opacity makes the spectral lines weak irrespective of the redistribution mechanism.

When only coherent electron scattering is present, the partial redistribution of the photons by atoms affects the wings of the lines. If continuous absorption is also present, the coherent electron scattering and the continuous absorption are the competing mechanisms which determine the shape of the lines. When the continuous absorption is more than the electron scattering, we get broader profiles irrespective of the redistribution mechanism. Partial redistribution by atoms gives shallower line profiles compared to coherent electron scattering.

The emission and absorption profiles are equal at the Doppler core even if stimulated emission is important. The deviation of the emission profile from the absorption profile is more for coherent type of redistribution. R_{III} redistribution can be approximated by complete redistribution for all practical purposes.

Even if small macroscopic velocities are present in the atmosphere, they affect the Ca II H and K lines. A single peaked emission instead of double peaked emission is obtained for K line when the velocity at the outer boundary of a schematic chromospheric type of atmosphere is one mean thermal unit. The small velocities do not produce any appreciable asymmetry in Ca II triplet lines.

6.2. Future work

So far we have considered only plane parallel atmospheres. When the thickness of the atmosphere is comparable to the radius of the star, the assumption of plane parallel atmosphere is not valid. Then we can represent the atmosphere as spherically symmetric medium to start with. A study of the effect of the redistribution functions on line formation in such atmospheres will throw more light on the spectra of giants and supergiant stars. One of the existing methods (Peraiah, 1972, Schmid-burgk, 1973, Hummer and Rybicki, 1971) to solve the transfer equation in such systems may be suitable for such a study.

The ultraviolet observations of spectral lines from early type stars suggest that the radiation driven winds may be present in these stars. The mass loss from these stars can be quantitatively studied in a consistent way only if we consider velocity fields in the regions of line formation. Now there is coupling between radiative transfer, statistical equilibrium, hydrodynamic, energy and momentum equations. The radiation and the velocity fields can be obtained in a consistent way only if we solve the above set of equations. As a first approximation, one can probably assume certain velocity laws and compute the radiation field. Even then it is very difficult to solve the transfer equation because the velocity fields in these stars exceed the sonic speed by

several times. Now the comoving frame transfer equation may come in handy and there are several existing methods to solve this equation (Mihalas et al 1976, Peraiah, 1980, Peraiah, 1985). The physical processes are easier to track in the comoving frame and by solving this equation one can get the source function values which can be substituted in the formal solution to obtain the fluxes in the observer's frame.

The redistribution functions for multi-level atom are derived by Hubeny (1981). A quantitative study ascertaining the effect of these on several lines which can be calculated simultaneously by considering multi-level atoms is another problem yet to be solved.

Line formation in turbulent media has many applications in the field of astrophysics. The treatment of this problem by Heidelberg group (1974) may be suitable for further study.

The parametric study provides us the information on the effect of each individual process. After such a study, it is easy to discriminate the unimportant physical processes from the important ones and selectively include them along with realistic model atmospheres and model atoms in the spectral line calculations, so that one can compare the theoretical results with the observations to derive some meaningful information. we propose to undertake some of the aforementioned problems in the future.

REFERENCES

- Abhyankar, K., 1964. Ap.J., **140**, 1353.
- Abramovitz, M., and I. Stegun., 1974. Handbook of Mathematical functions, Dover, New York.
- Adams, T.F., Hummer, D.G., Rybicki, G.B. 1971, J.Q.S.R.T., **11**, 1365.
- Ambartzumian, V.A., 1942. Russian Astron.J., **19**, 1.
- Arthur Schuster, 1905. Ap.J., **21**, 1.
- Athay, G.R., 1970, Sol.Phys., **11**, 347.
- Auer, L., and Mihalas, D., 1968. Ap.J., **153**, 245.
- Auer, L., and Mihalas, D., 1969. Ap.J., **158**, 641.
- Baschek, B., Mihalas, D., and J. Oxenius, 1981. Astron. astrophys., **97**, 43.
- Basri, G.S., 1979. Ph.D. Thesis, University of Colorado, Boulder.
- Basri, G.S., Linsky, J.L., Eriksson, K. 1981, Ap.J., **251**, 162.
- Chandrasekhar, S., In a discussion held at the Yerkes Observatory (unpublished).
- Chandrasekhar, S., 1950, Radiative transfer (Oxford: Oxford University press).
- Compton, 1923, Phil. Mag., **46**, 908.
- Dirac, P.A.M., 1925, M.N.R.A.S., **85**, 825.
- Dirac, P.A.M., 1958., The principles of quantum mechanics. Oxford: Clarendon press.
- Dumont, S. 1967., Annales d'Astrophysique, **30**, 421.
- Gebbie, K.B., and Thomas, R.N., 1968, Ap.J., **134**, 285.

- Giovenelli, R.G., 1967, Australian J. Phys., **20**, 81.
- Grant, I.P. and Hunt, G.E., 1969 a, Proc.R.Soc.A., **313**, 183.
- Grant, I.P. and Hunt, G.E., 1969 b, Proc.R.Soc.A., **313**, 199.
- Grant, I.P. and Peraiah, A., 1972. M.N.R.A.S., **160**, 239.
- Heidelberg group, Gail, H., Hundt, E., Kegal, W., Schmid, Burgk, J., and Traving, G., 1974. Astron. Astrophys, **32**, 65.
- Heinzl, P., 1981. J.Q.S.R.T., **25**, 483.
- Heinzl, P., and Hubeny, I., 1983. J.Q.S.R.T., **30**, 77.
- Henry, L.G., 1941. Proc.Nat.Acad.Sci., **26**, 50.
- Hubeny, I., 1981. Bull.Astron.Instit.Czech., **32**, 271.
- Hubeny, I., and Heinzl, P., 1984. J.Q.S.R.T., **32**, 59.
- Hummer, D.G., 1962. M.N.R.A.S., **125**, 21.
- Hummer, D.G., and Mihalas, D., 1967. Ap.J. Letters., **150**, L57.
- Hummer, D.G., 1969. M.N.R.A.S., **145**, 95.
- Hummer, D.G., and Rybicki, G., 1971. M.N.R.A.S., **152**, 1.
- Kalkofen, W., 1970. IAU Colloquium, 120.
- Kalkofen, W., 1974. Ap.J., **188**, 105.
- Kalkofen, W., 1984. editor, Methods in Radiative Transfer., Cambridge University press., London.
- Kulander, J., 1968. J.Q.S.R.T., **8**, 273.
- Linsky, J., 1969. Ph.D.Thesis. S.A.O. Special report no. **274**.
- Linsky, J., and Avrett, E., 1970. P.A.S.P. **82**, 169.
- Matta, F., and Reichel, A., 1971. Math.Comp., **25**, 339.
- Mihalas, D., 1978. Stellar atmospheres, 2 edn. Freeman, san Francisco.
- Mihalas, D., Kunasz, P., and Hummer, D.G., 1976. Ap.J. **210**, 419.

- Milkey,R., and Mihalas,D., 1973. Ap.J., **185**, 709.
- Milne,E.A., 1928. M.N.R.A.S., **88**, 493.
- Mohan Rao,D., Rangarajan,K.E., and Peraiah,A., 1984. J.Astrophys.Astron., **5**, 169.
- MUnch,G., 1948. Ap.J., **108**, 116.
- Omont,A., Smith,E., and Cooper,J., 1972. Ap.J., **175**, 185.
- Oxenius,J., 1965. J.Q.S.R.T., **5**, 771.
- Pasachoff, 1970. Sol.Phys., **12**, 202.
- Peach,G., 1967. Mem.R.A.S., **71**, 1.
- Peraiah,A., 1971. Ph.D. Thesis., Oxford University.
- Peraiah,A., 1978. Kodaikanal Obs. Bull. Ser. A,2, 115.
- Peraiah,A., 1980. J.Astrophys.Astron., **1**, 101.
- Peraiah,A., 1985. Private communication.
- Preisendorfer,R.W., 1965. Radiative transfer on discrete spaces. Oxford: Pergamon press.
- Rangarajan,K.E., Mohan Rao,D., and Peraiah,A., 1981. Kodaikanal Obs. Bull. Ser. A., **3**, 75.
- Redheffer,R.M., 1962. J.Math.Phys., **41**, 1.
- Shine,R., Milkey,R., and Mihalas,D., 1975. Ap.J.,**199**, 724.
- Steinitz,R., Shine,R.A., 1973. M.N.R.A.S., **162**, 197.
- Thomas,R.N., 1965. Some aspects of Non-equilibrium Thermodynamics in the presence of a radiation field. University of Colorado press, Boulder.
- Unno,W., 1952. P.A.S.J., **3**, 158.
- Van de hulst, 1963. Mem.soc.roy.Sci., Liege., **5,7, 78**.
- Vardavas,I.M., 1976 a. J.Q.S.R.T., **16**, 1.
- Vardavas,I.M., 1976 b. J.Q.S.R.T., **16**, 715.

Vardavas, I.M., 1976 c. J.Q.S.R.T., **16**, 781.

Wick, G.C., 1943. Zs.f.Physik., **120**, 702.

Wiese, W.L., Smith, M.W., and Miles, B.M., 1969. NBS Circular no. 22.

Wooley, R., and Stibbs, D., 1953. The outer layers of a star. Oxford: Clarendon press.